A Frequency Offset Lock for Cavity-Driven Raman Transitions

A diploma thesis submitted to the
Department of Experimental Physics,
University of Innsbruck

for the degree of
Master of Natural Science
(Magister Rerum Naturalium)

presented by
Thomas Monz

September 2005

In Gedenken unserer
"Haller Oma",
welche den Abschluss dieser Arbeit leider nicht mehr
erleben durfte.

Abstract

This thesis reports on the implementation of a frequency offset lock for a 854 nm laser system to investigate Raman passages in $^{40}Ca^{+}$ ions as single photon sources.

The circuit layout is discussed and crucial parameters explained. Measurements of the error signal depending on signal power and frequency were made. The linewidth of the offset laser is compared with estimations made by interpreting the noise on the error signal and other measurements on the offset laser system.

This tunable frequency offset lock has then been used to measure the length of a near concentric cavity, resulting in estimations of important parameters for the given experimental setup.

Contents

Dedication **III**

Abstract **V**

Contents **VII**

1 Introduction **1**
1.1 Motivation 1
1.2 Raman passages in an optical resonator 2

2 The interaction of light and atoms **5**
2.1 The two level system 5
2.2 The three-level system 10

3 State transfer in three level systems **13**
3.1 Incoherent excitation 14
3.2 Adiabatic Raman passage 14
3.3 Raman passage 17
3.3.1 AC-Stark shift during a Raman passage 18

4 Realisation of the 3 level model **21**
4.1 The $^{40}Ca^{+}$ ion as three level system 21
4.2 The ion trap 24
4.2.1 Laser cooling of trapped ions 27
4.3 The optical resonator 29
4.4 The compound system 34

5 Frequency offset lock **37**
5.1 Schemes 37
5.1.1 Frequency-to-voltage converters 39
5.1.2 Locking with a delay line 40
5.1.3 A high-pass filter as a frequency-to-voltage converter 42

5.2 Closing the locking loop - piezo and current control 44
5.2.1 Servo control of a piezo 44
5.2.2 Current control via a field-effect transistor 48

6 Experimental setup of the offset lock 51
6.1 Circuit layout 51
6.2 Frequency behaviour 54
6.3 Intensity dependence 56
6.4 Technical details of the combined locking setup 58
6.4.1 The reference laser at 854 nm 58
6.4.2 PID and Scan control of the Toptica DL100 system 58
6.4.3 Additional current control through a FET 60
6.5 Linewidth of the locked laser 60
6.6 Optical setup of the offset lock on the breadboard 64
6.7 Limiting factors 65
6.7.1 A single-sideband mixer 65
6.7.2 Reducing intensity fluctuations 67

7 Applications of the offset lock in the experiment 69
7.1 Frequency pointer 69
7.1.1 Mode spectrum of a cavity 70
7.1.2 Measurement results of the cavity length 72

8 Conclusions and outlook 77

Bibliography 79

Acknowledgements 83

Curriculum Vitae 85

Chapter 1

Introduction

1.1 Motivation

Physics tries to describe the world by using small, calculable parts, and using them to describe more complex processes by putting these small parts together and looking at their interaction.

Obviously, atoms and light are very basic systems that need to be understood as well as possible to be able to make predictions about processes in nature.

Cavity quantum electro dynamics (CQED) is a branch of physics dealing with exactly these two topics at a very basic level. The interaction of single atoms with single modes of quantised light is investigated, revealing interesting new interactions like stimulated Raman adiabatic passage (STIRAP). The basic theory of atom–light interaction was developed by Jaynes and Cummings in 1963 [1], and was complemented in 1970 by Stehle [2] and Barton [3]. Huge amounts of experimental and theoretical work have been added since then on these very basics of nature.

This knowledge allows state preparation and manipulation to an extent that results in 'on demand' state shaping. Looking forward to implement computation on an atomic level, these tools provide the needed basics to achieve such demanding goals.

In 2000, DiVincenzo [4] discussed several requirements that have to be fulfilled for the implementation of quantum computation, and included two more requirements relating to the sharing of information via quantum communication. The requirements for quantum computation are:

- A scalable physical system with well characterised quantum bits (qubits).
- The ability to initialise the state of the qubits to a simple fiducial state, such as $|000\rangle$.
- Long relevant decoherence times, much longer than the gate operation.

- A "universal"set of quantum gates.
- A qubit-specific measurement capability.

To be able to use quantum mechanics to its full possibilities, quantum information processing and computation should fulfil two more criteria as basics for quantum communication:

- The ability to interconvert stationary and flying qubits
- The ability to faithfully transmit flying qubits between specified locations.

It has been shown, that, alongside research areas in physics like superconducting devices, quantum dots, electron physics and many others, trapped ions strings are a promising field to investigate the possibilities of quantum computation [5, 6] as they fulfil all needed criteria. The information in these systems is stored by using the ground state and an other long lived excited state of single atoms as qubits.

Trapped ions fulfil the first five criteria of DiVincenzo, but do not present a possibility to convert stationary qubits into flying qubits. Our goal is to use the well known and excellent properties of trapped ions and combine them with a high finesse cavity.

Coupling the stored ions to the cavity field will allow the conversion of stationary qubits into flying qubits, as the photon emitted during an atomic state change will be collected by the cavity. Coupling the cavity output field to a fiber would finally result in fulfilling the additional two criteria mentioned by DiVincenzo.

1.2 Raman passages in an optical resonator

A possible approach to the transfer of information from a stationary qubit into a flying qubit is to perform an adiabatic or ordinary Raman passage on an ion that is described by a three level system. To collect the single photon produced during such a population transfer from the ground to the excited state, the electric field of the second laser that is normally used to describe these transitions in theory is replaced by the field of a high finesse cavity. This replacement is valid and easily done in theory, as the mathematics describing a light field stays the same for a laser as for the field stored in an optical resonator. The formulae can be easily changed according to the slightly different physics. Performing the transition from the ground to the excited state results in a single photon in the cavity mode. This photon represents the information of the prior stationary qubit, the atom, now as a flying qubit, a photon. This photon can be used to transfer the information of the first qubit, the atom, to another quantum system. By shaping the wavepacket of

the photon, one can even ensure unity transmission into another ion-cavity system with a coupled ion[7].

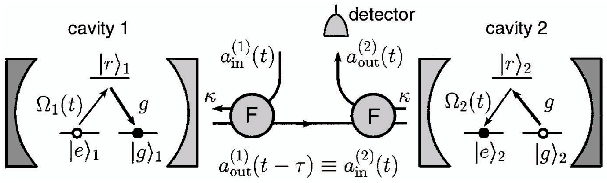

Figure 1.1: A possible way of connecting separated quantum systems, presented in [7]

The whole setup represents a possible scheme of a quantum network, allowing quantum computation at different nodes with trapped ions, while being able to perform sharing of quantum information between distant nodes via photons.

An optimal photon production relies on the coherent population transfers between the used states in the atoms. Since decay by spontaneous emission from an excited state is inherent in any atomic system, frequency offsets to the atomic transitions are used to reduce the effective decay rates of the pseudo two level system derived from idealised lambda systems in the underlying theory.

This thesis reports on an approach using a high–pass filter technique to produce such a frequency offset lock on an atomic transition. The light will be used as a frequency pointer to stabilise the cavity of the experimental setup to the right distance. Assessments about advantages and limits of this scheme, as well as the achievable parameters of the experimental cavity setup are presented.

Chapter 2

The interaction of light and atoms

2.1 The two level system

An atom consists of a positively charged nucleus and one or more (negatively charged) electrons, which are bound to the core through the Coulomb force. The bound electron(s) can have several different states, depending on the energy of the electron, the applied magnetic and/or electric fields, and other factors.

The most simple model for an atom is to think of a two-level system. The electron is in either the ground ($|g\rangle$) or excited ($|e\rangle$) state. In analogy with a 'bit', the binary digit in computer systems, these states can be labelled 0 and 1. The atom is going to interact with a light field and possible interactions will be explained.

The time-dependent state of the system is given by:

$$|\psi\rangle = \alpha(t)|g\rangle + \beta(t)|e\rangle \tag{2.1}$$

where $\alpha(t)$ and $\beta(t)$ resemble the time-dependent population of the ground and excited state, with the condition $|\alpha(t)|^2 + |\beta(t)|^2 = 1, \forall t$.

In matrix notation the states of the system are given by:

$$u(g) = \begin{pmatrix} 0 \\ 1 \end{pmatrix}, u(e) = \begin{pmatrix} 1 \\ 0 \end{pmatrix} \tag{2.2}$$

The energy difference of the two states is defined as $\hbar\omega_0$. The zero energy point is defined to be exactly in the middle of the two states (see Figure 2.1 on the following page), which gives the following description of the energy of the system:

$$\hat{H}_{atom} = -\frac{1}{2}\hbar\omega_0 \begin{pmatrix} 1 & 0 \\ 0 & -1 \end{pmatrix} = -\frac{1}{2}\hbar\omega_0\sigma_z \tag{2.3}$$

The electric field of light can be described by a superposition of harmonic oscillators. As the experimental setup is designed in such a way that only one mode

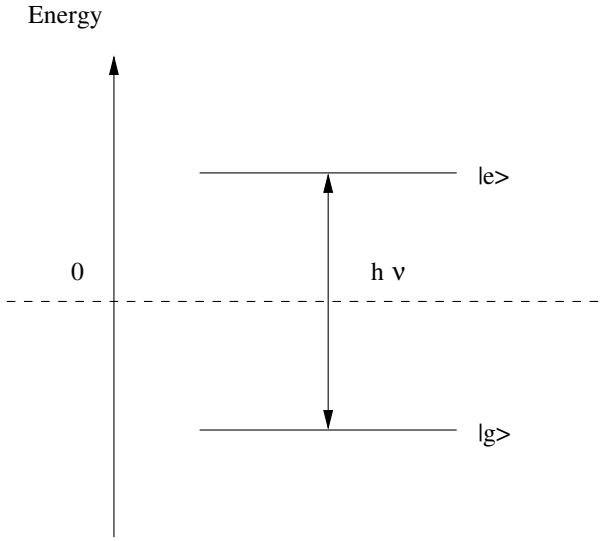

Figure 2.1: The energy levels of the two level system, according to the presented theory. The zero energy level is chosen to be exactly in the middle between the two states, representing the energy model of a spin as an analogy to a quantum or classical bit

of the cavity will couple effectively to the atom, the field of the light is described by only one frequency ω.

The Hamilton operator of a one-dimensional oscillator is given by:

$$\hat{H}_{field} = \hbar\omega(\hat{a}^\dagger\hat{a} + \frac{1}{2}) \tag{2.4}$$

The interaction of the electric field of the light with an atom to perform dipole transitions can be described by the interaction Hamiltonian:

$$\hat{H}_{inter} = \vec{\mu}\vec{E}(\sigma^+ + \sigma^-) \tag{2.5}$$

$\vec{\mu}$ is equivalent to the dipole, being an expectation value that represents how well these two states can be used in order to perform dipole transitions induced by the coupling between the electrical field and the atom. For a single electron, this is equal to $e \cdot \vec{r}$, the location of the electron.

$$\vec{\mu} = e\langle g|\vec{r}|e\rangle \tag{2.6}$$

σ^+ and σ^- represent the state interaction, from the ground to the excited, and from the excited to the ground state. In matrix formalism, this is written:

$$\sigma^+ = \begin{pmatrix} 0 & 1 \\ 0 & 0 \end{pmatrix}, \sigma^- = \begin{pmatrix} 0 & 0 \\ 1 & 0 \end{pmatrix} \tag{2.7}$$

$\vec{E}$ is the field operator of the electric field. Quantising the electric field, each mode of a free running wave corresponds to a quantum mechanical oscillator of the form:

$$\hat{E} = i\sqrt{\frac{\hbar\omega}{2\varepsilon_0(2\pi)^3}}\vec{\epsilon}\{\hat{a}\exp(-i\omega t + i\vec{k}\cdot\vec{r}) - \hat{a}^\dagger\exp(i\omega t - i\vec{k}\cdot\vec{r})\} \tag{2.8}$$

$\vec{\epsilon}$ is the unit vector that describes the polarisation and $a^\dagger$ and a are annihilation and creation operators of the field. A light source is described by summing over all modes and polarisations, and integrating over all frequencies.

This description changes slightly for the lightfield in a cavity to a [8]

- single mode standing wave:

$$\hat{E} = i\sqrt{\frac{\hbar\omega}{2\varepsilon_0 V}}\vec{\epsilon}\{(\hat{a} - \hat{a}^\dagger)\sin(kz)\} \tag{2.9}$$

- single mode running wave in a ring cavity:

$$\hat{E} = i\sqrt{\frac{\hbar\omega}{2\varepsilon_0 V}}\vec{\epsilon}\{\hat{a}\exp(i\vec{k}\vec{r}) - \hat{a}^\dagger\exp(-i\vec{k}\vec{r})\} \tag{2.10}$$

with V being the mode volume of the cavity.

The light field will be split into two parts:

$$\hat{E} = \mathcal{E}(t)\vec{\epsilon}\exp(-i\omega t) + c.c. = E^{(+)} + E^{(-)} \tag{2.11}$$

where $\mathcal{E}(t)$ is varying slowly on the optical time scale. This way of describing the light is in terms of the annihilation or creation associated with the terms of $\exp(\pm i\omega t)$. This allows a straightforward look at the different terms of the interaction.

The combined Hamiltonian for a two level system interacting with a single–mode light field is:

$$\hat{H} = \hat{H}_{\text{atom}} + \hat{H}_{\text{field}} + \hat{H}_{\text{inter}} \tag{2.12}$$

where $\hat{H}_{\text{atom}}$ and $\hat{H}_{\text{inter}}$ have the form described above, and the Hamiltonian of the light field $\hat{H}_{field}$ is the energy of one photon times the number of photons present, resulting in $\hat{H}_{\text{field}} = \hbar\omega a^\dagger a$. The additional term $+\frac{1}{2}\hbar\omega$ has been dropped, as it constant and has no influence on the behaviour of the system.

For further simplification, the dependency of the field on the location of the atom is neglected, since the atom will be very well localised in the trap and the atom is small in comparison to the wavelength ($a_{Bohr}/\lambda \approx 10^{-4}$). So we ignore the $\vec{k}\cdot\vec{r}$ term by setting it to zero, which is called "dipole approximation".

Another approximation that will be applied later to this theory is the rotating-wave-approximation (RWA). It takes the different timescales into account. Looking at the occurring frequencies ω and ω_0, there is the sum and difference between

the 2 frequencies. The argumentation is, that terms oscillating with the sum of the frequencies 'blur out' during the much slower interaction were the difference frequencies occur. This approximation is reasonable once you compare the timescale of the transfer and the laser: A transfer takes place in roughly 10^{-7} s, while the light field oscillates at a timescale of 10^{-15} s.

One derives a two-level system coupled to a quantised harmonic oscillator, the Jaynes-Cummings model.

Expanding the interaction Hamiltonian shows the possible transition from the ground to the excited state while emitting a photon. The opposite process is represented by a term equal to absorbing a photon while changing from the excited to the ground state. These two terms will be neglected due to very small probability of occurency because of the break of energy conservation. It can be shown that this simplification is valid as long as the interaction energy is much smaller than the energy of the photon or transition energy.

The simplified interaction Hamiltonian is then given by:

$$\hat{H}_{\text{inter}} = \hbar\mu\{\hat{a}\sigma^- E^{(+)} + \hat{a}^\dagger\sigma^+ E^{(-)}\} = \frac{1}{2}\hbar\Omega\{\hat{a}\sigma^- \exp(-i\omega t) + \hat{a}^\dagger\sigma^+ \exp(i\omega t)\} \quad (2.13)$$

with the Rabi frequency:

$$\Omega = \frac{2\mathcal{E}\vec{\mu}}{\hbar} \quad (2.14)$$

This will be the frequency at which the population will coherently swap between ground and excited state for coherent excitation.

The presented interaction Hamiltonian has a simple physical interpretation. Excitation of the atom requires the loss of a photon from the cavity mode, and the transition of the atom from excited to ground state is accompanied by the emission of a photon.

Consider only the Hamiltonian of the atom and the atom-light interaction:

$$\hat{H} = \frac{1}{2}\hbar \begin{pmatrix} -\omega_0 & \Omega\exp(i\omega t) \\ \Omega\exp(-i\omega t) & \omega_0 \end{pmatrix} \quad (2.15)$$

The parameters in the Hamiltonian depend on the chosen basis. Moving to a rotating basis we eliminate the oscillating terms:

$$H_I = \hbar \begin{pmatrix} 0 & \frac{\Omega}{2} \\ \frac{\Omega}{2} & \Delta \end{pmatrix} \quad (2.16)$$

where $\Delta = \omega_0 - \omega$, the detuning of the light from the atomic transition, i.e. a positive (negative) detuning denotes red– (blue–) detuned light.

This simple Hamilton operator contains all the information needed to calculate the time evolution of the system for given start parameters via the Schrödinger

equation $i\hbar\frac{\partial}{\partial t}|\psi\rangle = H|\psi\rangle$. This equation can be solved analytically. The evolution of the population of the excited state (with no population in the excited state at $t = 0$) is:

$$\rho_{22}(t) = \frac{\Omega^2}{\Omega'^2}\sin^2(\frac{1}{2}\Omega' t) \tag{2.17}$$

$$\Omega' = \sqrt{\Delta^2 + \Omega^2} \tag{2.18}$$

The effective Rabi frequency depends on the detuning of the light field. As the detuning increases, the maximal population of the excited state is reduced, while the frequency of the Rabi oscillations increases. These effects can be seen in Figure 2.2.

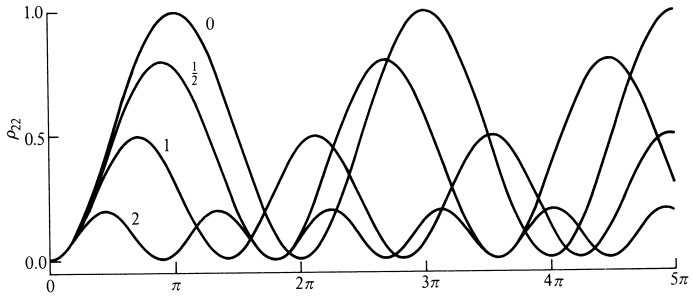

Figure 2.2: Rabi oscillations without damping: The x axis is given in units of Ωt, while the probability to find the two level system in the excited state is shown on the y axis. The numbers next to the plotted lines indicate the detuning divided by the Rabi frequency $(\omega_0 - \omega)/\Omega$. For larger detunings, the increasing effective Rabi frequency and the smaller excitation probability is clearly visible. Taken from [9]

An interesting case is of light with a wavelength of the exact transition wavelength. For such resonant light, population can be moved from the ground state to the excited state in an alternating way. In other terms, the atomic bit can be flipped from $|0\rangle$ to $|1\rangle$ and back as much as desired.

However, this description describes an idealised system. All excited states in an experiment will decay by spontaneous emission of light. It is experimentally impossible to exclude spontaneous emission of light, therefore it must also be included in the theory.

In the absence of an electric field, decay from the excited state can be introduced into the Hamiltonian, resulting in an exponential decay of the excited state equal to $\rho_{22}(t) = \rho_{22}(0)\exp(-\gamma t)$. While for amplitudes γ is often used, for population decays $\Gamma = 2\gamma$ is used. This term can be understood as damping of the oscillations.

$$H_I = \hbar \begin{pmatrix} 0 & \frac{\Omega}{2} \\ \frac{\Omega}{2} & \Delta - i\gamma \end{pmatrix} \tag{2.19}$$

An analytical expression for the evolution of the excited state in a two level system, driven with resonant light and including spontaneous decay (starting at $t = 0$ with no population in the excited state) is given by:

$$\rho_{22}(t) = \frac{\frac{1}{2}\Omega^2}{2\gamma^2 + \Omega^2}\left\{1 - \left[\cos(\lambda t) + \frac{3\gamma}{2\lambda}\sin(\lambda t)\right]\exp(-3\gamma t/2)\right\} \tag{2.20}$$

where

$$\lambda = \sqrt{\Omega^2 - \frac{1}{4}\gamma^2} \tag{2.21}$$

Figure 2.3 shows that spontaneous decay severely limits the possibility of switching between the ground and the excited state on a larger timescale.

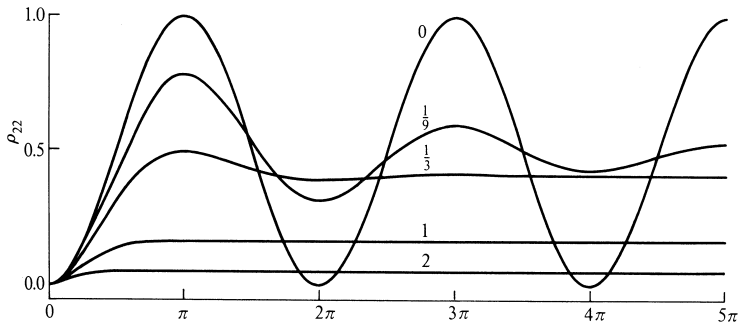

Figure 2.3: Rabi oscillations for resonant excitation with damping: The numbers next to the lines represent the ratio of radiative damping γ to Rabi frequency Ω. Taken from [9]

2.2 The three-level system

The coherence time of a two level system depends on the life time of the excited state. Adding another long lived level to this system may allow the coupling of the ground state with the long lived state in order to obtain a longer coherence time.

A three-level system can have one of three level schemes. These are called Ξ, V and Λ schemes, and are shown in figure 2.4 on the next page. There are 3 states, with state $|1\rangle$ coupling to state $|2\rangle$, and state $|2\rangle$ coupling to state $|3\rangle$. Spontaneous decay couples the same transitions. We consider here only these three schemes where state $|1\rangle$ and state $|3\rangle$ are not coupled.

The first scheme, Ξ, is a ladder system. In the absence of decay, the population can be moved from $|1\rangle$ to $|3\rangle$ with resonant light [10], however the inclusion of decay results in a lack of states between that populations can be coherently moved.

The second layout consists of two excited states and one ground state. This system can also be thought of as two two-level-systems, sharing a single groundstate.

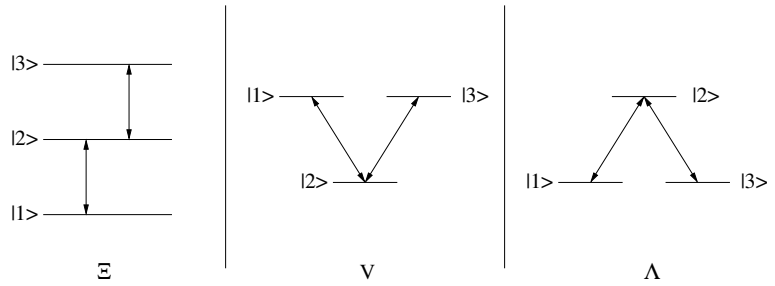

Figure 2.4: Schematics of 3 level systems. The connections between the states represent the transitions and decay channels that are normally included in a theoretical treatment.

Although unsuitable for our purposes (since both states $|1\rangle$ and $|3\rangle$ decay), this system allows the interesting possibility of measuring quantum beats and quantum jumps.

Finally, the Λ system consists of 2 ground states and one excited state. In analogy to a classical bit, the two groundstates could be labelled 0 and 1, without losing population in these states as a result of spontaneous decay.

Movement of the population between the ground states while being able to neglect the presence of the excited state gives an effective two level system with nearly no decay, and opens up the possibility of using this configuration for quantum computation.

Chapter 3

State transfer in three level systems

As described in section 2.2 on page 10, a pseudo two level system without decay may be derived from a three level system in lambda assembly.

The following chapter will explain in more detail how this works and gives some information about the requirements that must be fulfilled in order to obtain the desired two-level system.

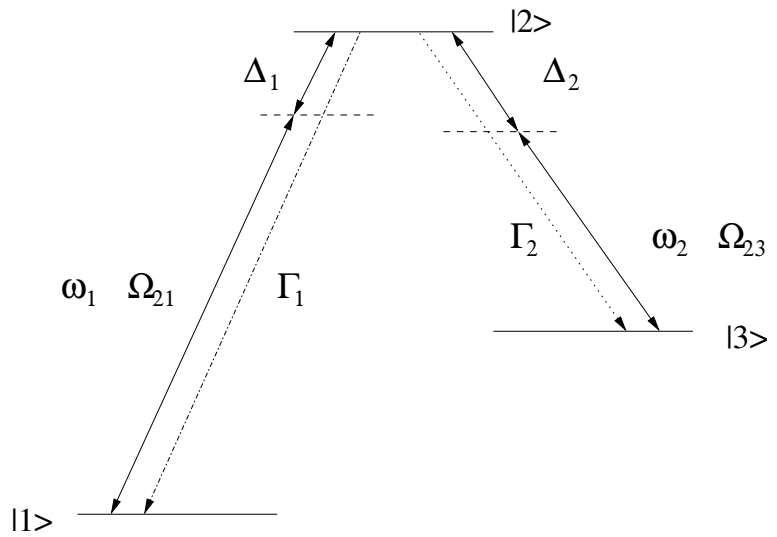

Figure 3.1: Definitions of the variables used for describing the lambda system: Δ represents the offset from the atomic transition, Ω is the Rabi frequency resulting from the field atom interaction. $\Gamma_{1,2}$ is the decay rate of the excited state $|2\rangle$ into the according states $|1\rangle$ and $|3\rangle$.

Different population transfers in this system will be described. Starting with population in state $|1\rangle$, this population can, e.g. be transferred, by performing a Rabi flop on the $|1\rangle$–$|2\rangle$ transition, and transfering the population to state $|2\rangle$. From there, one can either perform a second Rabi flop on the $|2\rangle$–$|3\rangle$ transition or just

wait until a part of the population decays into state $|3\rangle$.

Another possibility is to shine light resonant on both transitions simultaneously. The coupling between state $|1\rangle$ and $|3\rangle$ via $|2\rangle$ will result in population transfer.

All these procedures are affected by decoherence, as spontaneous decay from state $|2\rangle$ is present. Having a closer look at a feature of population transfer with 2 laser beams shining on the atom, the theory of performing a stimulated adiabatic Raman passage (STIRAP) is discussed.

Due to the adiabaticity of the STIRAP process and the therefore slow population transfer, a Raman passage is discussed as a resonant two photon transition from state $|1\rangle$ to $|3\rangle$.

3.1 Incoherent excitation

One obvious way to move a population from state $|1\rangle$ to state $|3\rangle$ is to apply resonant light on the $|1\rangle$–$|2\rangle$ transitions and wait until some population is transferred into state $|3\rangle$ by spontaneous decay from state $|2\rangle$. This probabilistic state transfer is not desired as a tool for coherently transfer atomic state information into a photon. On this account, this population transfer will not be discussed further.

Another way is to move population again to state $|2\rangle$ by a Rabi flop, and then perform a second Rabi flop on the $|2\rangle$–$|2\rangle$ transition. Although this represents a possibility to transfer larger amounts of population into state $|3\rangle$, during this process state $|2\rangle$ has to be populated once. This immediately leads to decoherence as this state decays.

Another scheme is to shine light on both transitions at the same time. The idea is to move population in state $|2\rangle$ directly into state $|3\rangle$, and suppressing decoherence by a short population time of state $|2\rangle$. The time dependence of state populations during such a procedure is shown in figure 3.2 on the next page. Again, any population in state $|2\rangle$ leads to decoherence. Therefore the idea is to search for transitions, that do not populate state $|2\rangle$.

An interesting feature is that this population transfer results in a residual population in state $|1\rangle$, that does not seem to couple to the applied light (compare with the population probability after a long time scale). This detail will be discussed in the following, leading to the possibility to move population adiabatically from state $|1\rangle$ to state $|3\rangle$, without populating state $|2\rangle$.

3.2 Adiabatic Raman passage

In order to understand, why a portion of the ground state population doesn't seem to couple to the applied light, more theory has to be presented to give an understanding

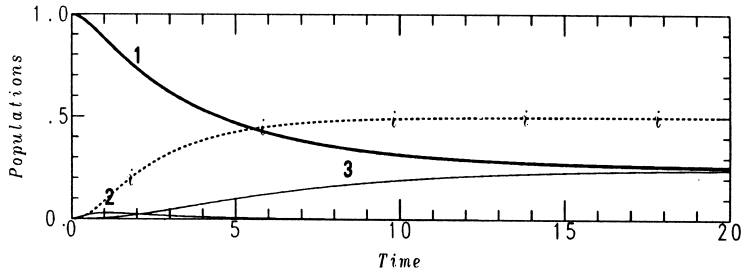

Figure 3.2: Solving the time evolution of a system described by equation 3.1, a population history $P_n(t)$ for a resonantly excited λ system, with $\Omega_{21} = \Omega_{23} = 1$ and $\gamma = \frac{5}{2}$, is derived [10].

of the underlying physics.

The Hamiltonian for the 3 level system (with rotating wave approximation [10]) is given by:

$$H_\Lambda = \hbar \begin{pmatrix} \Delta_1 & \frac{\Omega_{12}}{2} & 0 \\ \frac{\Omega_{12}}{2} & -i\gamma & \frac{\Omega_{23}}{2} \\ 0 & \frac{\Omega_{23}}{2} & \Delta_3 \end{pmatrix}, \tag{3.1}$$

with the following definitions:

$$\hbar\Delta_1 = -(E_2 - E_1) + \hbar\omega_1 \tag{3.2}$$

$$\hbar\Delta_3 = -(E_2 - E_3) + \hbar\omega_2 \tag{3.3}$$

and Ω according to Equation 2.14 on page 8. Hereby the zero energy level is chosen to be equal to the energy of state $|2\rangle$.

We consider first the resonant case, $\Delta_1 = \Delta_2 = 0$. The eigenvalues of the Hamiltonian can be calculated and correspond to zero and the eigenvalue of a two-level system with damping, with a Rabi frequency of

$$\bar{\Omega} = \sqrt{(\Omega_{21})^2 + (\Omega_{23}^2)} \tag{3.4}$$

The presence of an eigenvalue of zero (or more generally, an eigenvalue with no imaginary part) hints at the possibility of a non-decaying eigenmode.

Changing to another basis, with a coherent superposition of states according to:

$$\Phi_+(t) = \{\Omega_{21}|1\rangle \exp(i\omega_1 t) + \Omega_{23}|3\rangle \exp(i\omega_2 t)\} / \bar{\Omega} \tag{3.5}$$

$$\Phi_-(t) = \{\Omega_{23}|1\rangle \exp(i\omega_1 t) - \Omega_{21}|3\rangle \exp(i\omega_2 t)\} / \bar{\Omega} \tag{3.6}$$

the system is described by

$$\Psi(t) = C_+(t)\Phi_+(t) + c_2(t)|2\rangle + C_-(t)\Phi_-(t) \tag{3.7}$$

with

$$C_+(t) = \left[\Omega_1 C_1(t) + \Omega_2 C_3(t)\right]/\bar{\Omega} \tag{3.8}$$

$$C_-(t) = \left[\Omega_2 C_1(t) - \Omega_1 C_3(t)\right]/\bar{\Omega} \tag{3.9}$$

resulting in the Hamiltonian

$$H' = \begin{pmatrix} \frac{\Delta_1\Omega_1^2+\Delta_3\Omega_2^2}{\Omega^2} & i\frac{\bar{\Omega}}{2} & (\Delta_1-\Delta_3)\frac{\Omega_1\Omega_2}{\Omega^2} \\ \frac{\bar{\Omega}}{2} & -i\gamma & 0 \\ i(\Delta_1-\Delta_3)\frac{\Omega_1\Omega_2}{\Omega^2} & 0 & \frac{\Delta_1\Omega_2^2+\Delta_3\Omega_1^2}{\Omega^2} \end{pmatrix} \tag{3.10}$$

For equal detunings (meaning that the difference in photon energies are equal to the energy difference between $|1\rangle$ and $|3\rangle$, or in other words equal to a resonant two photon transition between state $|1\rangle$ and $|3\rangle$), this results in a time evolution of the system $(|\Phi_+\rangle, |2\rangle, |\Phi_-\rangle)$ of:

$$H' = \begin{pmatrix} \Delta & \frac{\bar{\Omega}}{2} & 0 \\ \frac{\bar{\Omega}}{2} & -i\gamma & 0 \\ 0 & 0 & \Delta \end{pmatrix} \tag{3.11}$$

Within this Hamiltonian matrix a sub-matrix can be identified that represents a two level system with loss, given by the basis vectors $|\Phi_+\rangle$ and $|2\rangle$ (compare with equation 2.19 on page 9). The state $|\Phi_-\rangle$ is decoupled from the pseudo two level system, and evolves independently from the other states without decay.

An important point is, that for equal detunings, $|\Phi_-\rangle$ does not couple to $|\Phi_+\rangle$ as can be seen in equation 3.10. If this condition is not fulfilled, $|\Phi_-\rangle$ couples indirectly to $|2\rangle$ through $|\Phi_+\rangle$, which destroys the coherence.

Now consider the non-decaying eigenstate of the system. As described by equation 3.5 on the previous page, $\Phi_-(t)$ is a superposition of $|1\rangle$ and $|3\rangle$. Starting with all population in $|1\rangle$, the initial conditions are:

$$C_1(t=0) = 1, C_2(t=0) = 0, C_3(t=0) = 0 \tag{3.12}$$

With these starting parameters for the system, the coefficients for the new basis can be written:

$$C_+(t=0) = \sin(\theta), C_2(t=0) = 0, C_-(t=0) = \cos(\theta) \tag{3.13}$$

where θ is defined by:

$$\tan(\theta) = \frac{\Omega_{21}}{\Omega_{23}} \tag{3.14}$$

As one would like to have as much population as possible in state $|\Phi_-\rangle$, and looking at equation 3.13, an angle θ equal to zero needs to be obtained as a start

parameter. This can be achieved by starting with a much greater laser intensity in the transition between the unpopulated state $|2\rangle$ and $|3\rangle$ than on the transition between $|2\rangle$ and $|1\rangle$. This is counterintuitive, as states need to be coupled before they are even populated.

With all population in $|\Phi_-\rangle$, Ω_{21} and Ω_{23} can be adiabatically changed and the state will follow the change without losing population into the other states. Increasing Ω_{21} and reducing Ω_{23} results in a population transfer from $|1\rangle$ to $|3\rangle$ within the state $|\Phi_-\rangle$ without destroying it.

As shown in ref. [11], the adiabaticity condition is if the angle θ changes slowly compared to the splitting of the energies between the states. This is equivalent to the condition [12]:

$$\left|\frac{\dot{\Omega}_{21}\Omega_{23} - \Omega_{21}\dot{\Omega}_{23}}{\bar{\Omega}^2}\right| \ll \sqrt{\Delta^2 + \bar{\Omega}^2} \tag{3.15}$$

For small detunings, the Rabi frequencies determine the timescale that allow adiabatic passage. For large detunings, the eigenvalues that produce this condition, have to be considered. Far-off resonance conditions result in a very small energy difference between the nondecaying state and state $|2\rangle$, which can therefore easily couple. For that reason, one has to perform the passage very slowly to fulfil the adiabatic condition. Therefore performing adiabatic passage with large detunings is not optimal.

As previously mentioned, all of these calculations assume a perfectly resonant two–photon transition, in order to have no indirect coupling between $|\Phi_-\rangle$ and $|2\rangle$. Ref. [13] shows that even the slightest detuning, which is inevitable in an experiment, will cause an avoided crossing between state $|1\rangle$ and $|3\rangle$. This means, one starts in state $|1\rangle$, expressed in terms of $|\Phi_-\rangle$, which evolves slowly towards state $|3\rangle$, but realigns rapidly back into the eigenvector $|1\rangle$ (for more details see ref. [13]).

Adiabatic passage has nevertheless been demonstrated in experiments. The reason that this is possible is, that detunings smaller than the Rabi frequency result in a diabatic transfer at the avoided crossing, leading to the desired population transfer. This condition implies that detunings of the same sign for Δ_1 and $\Delta_1 - \Delta_2$, with Δ_1 smaller than $\Delta_1 - \Delta_2$, should be avoided.

In an experimental setup this is achieved by keeping the detunings as small as possible, with $|\Delta_1|$ not lying between zero and $|\Delta_1 - \Delta_2|$.

3.3 Raman passage

Considering again a two level system, the whole population can be moved from the ground to the excited state by applying resonant light for a time duration of $\tau = \frac{\pi}{\Omega}$. This is known as a π pulse.

Detuning the lasers far from the atomic transitions to state $|2\rangle$, this state can be neglected. The reason for this is the small population that can be found in this state due to the large detuning, as the probability to find the atom in state $|2\rangle$ approximately decreases for large detunings like $\frac{\Omega^2}{\Delta^2}$ (compare with equation 2.17 on page 9).

By neglecting the presence of state $|2\rangle$, a two level system is obtained. Perturbation theory predicts an effective coupling between the two states with a Rabi frequency of [14]:

$$\Omega_{\text{eff}} = \frac{\Omega_{21}\Omega_{23}}{2\Delta_1} \tag{3.16}$$

The effective decay rate can be described by [15]:

$$\Gamma_{\text{eff}} = \Gamma\frac{\Omega_{21}^2}{4\Delta_1^2} \tag{3.17}$$

with Γ being equal to the sum of decay rates of state $|2\rangle$. These equations assume large detunings compared to the Rabi frequencies. More detailed information can be found in ref. [16].

Although the effective Rabi frequency decreases as $\frac{1}{\Delta_1}$ for larger detunings, the spontaneous decay rate decreases as $\frac{1}{\Delta_1^2}$, allowing effective suppression of this source of decoherence.

3.3.1 AC-Stark shift during a Raman passage

The coupling of the laser fields with state $|2\rangle$ results in an AC-Stark shift of the level. For $\Omega_{21} \gg \Omega_{23} \gg \Gamma$, the splitting is equal to [17]:

$$\Delta_{AC\pm} = \frac{1}{2}(\Delta_1 \pm \sqrt{\Delta_1^2 + \Omega_{21}^2}) \tag{3.18}$$

For large detuning $\Delta_1 > \Omega_{21}$, the additional shift can be approximated with $\Omega_{21}^2/2\Delta_1$. The validity of this approximation will be justified later by comparing these parameters with the experimentally achievable parameters in our experiment.

Setting the detuning of the second laser to be resonant with the AC-Stark-shifted level, the desired two-level system is obtained, with small spontaneous decay and the possibility of performing a π pulse to move the whole population from state $|1\rangle$ to state $|3\rangle$.

Compared to the STIRAP, the Raman passage can create a single photon on a much shorter time scale. Figure 3.4 on the facing page illustrates the time evolution of between the two processes. Although the effective Rabi frequency is reduced for larger detunings, the necessity to adiabatically change the coupling strengths for the two arms in a STIRAP scheme normally results in less photons produced per time unit. Further research and comparison has been performed by Maurer in 2004 [15].

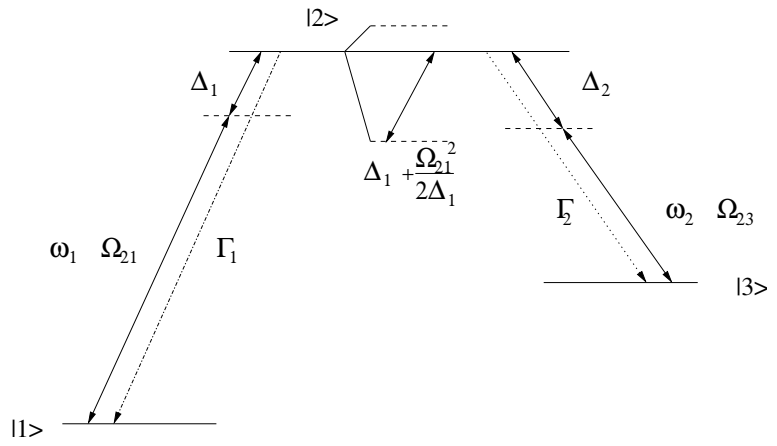

Figure 3.3: AC-Stark shifting of state $|2\rangle$. This shift needs to be taken into account in creating a resonant two–photon transition from state $|1\rangle$ to $|3\rangle$

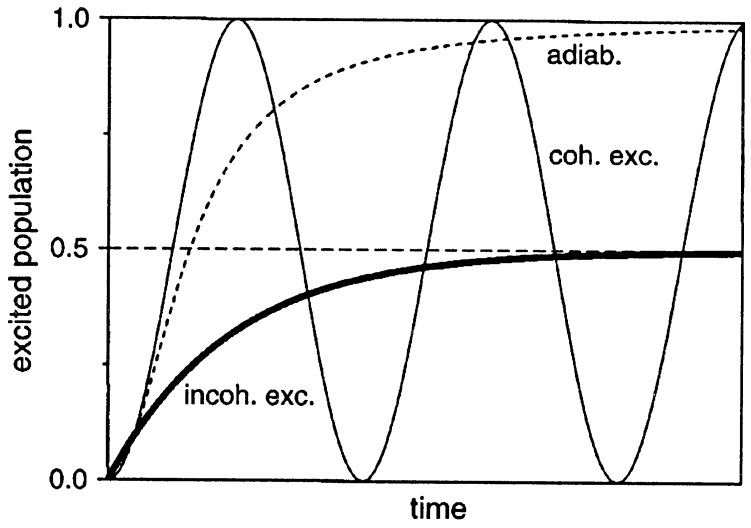

Figure 3.4: Evolution of the excited state in a two-level system, driven by an incoherent radiation field (heavy line), an adiabatic passage (dashed line) and by a coherent radiation field (thin line) [11]. Rabi oscillations can be performed on a much shorter timescale, depending only on the coupling strength, while the adiabatic passage requires the slow ramping of the coupling strengths of the two transitions.

This two-photon transition creates a photon in the second laser field. By replacing the second laser with a cavity that is stabilised to this wavelength, and spatially arranged in such a way that the atom can couple strongly to the field in the resonator, the photon is generated in the cavity mode. This cavity mode represents then the information of the state of the atom, as the stationary qubit from the atom was transferred into a flying qubit in the cavity. With one mirror of slightly smaller reflectivity, this information can be coupled out of the cavity via a photon and be sent to another quantum system. At this point it should be added, that the information about the atomic qubit is lost during this process.

The experimental challenge is to achieve a coupling between the cavity mode and the idealised three level system that is strong enough to be used for this transition. At the same time, processes such as the leaking of photons out of the cavity or the emission of photons outside of the cavity mode must be minimised.

Chapter 4

Realisation of the 3 level model

The previous chapters described how an effective two level system with a small decay rate is a suitable system to implement bit flips from classical computation into a quantum world by using a 3 level system with laser detuned from the atomic transitions and performing π pulses with a Raman passage. Later on, the photon produced during the population transfer will be coupled to a cavity, representing the transformation from a stationary to a flying qubit.

The current chapter will explain how this theoretical model is realised in our experiment, with $^{40}Ca^{+}$ ions. The ions level scheme is presented and the laser fields required to convert this complex structure to an effective three-level system are described.

This ion is spatially confined in a linear ion trap. The principle behind such trapping will be briefly introduced. Doppler and sideband cooling will be briefly explained to justify the previous assumption that the location of an ion is well-defined compared to the wavelength of the applied light. The optical resonator around the ion trap will then be explained. Properties of the resonator are presented and an overview of the process of collecting the single photons created during the Raman passage, is given.

Finally the compound system will be described.

4.1 The $^{40}Ca^{+}$ ion as three level system

Pure calcium is a silver-white light metal, that changes its colour to white due to oxidation if exposed to air. 96.9% of ordinary calcium consists of the nuclear spinfree isotope ^{40}Ca. A singly-ionised calcium atom can be represented as an argon electron configuration with an additional valence electron. Figure 4.1 on the next page shows the five lowest levels of the $^{40}Ca^{+}$ ion. Precise transition wavelengths and lifetimes of the states are given in table 4.1.

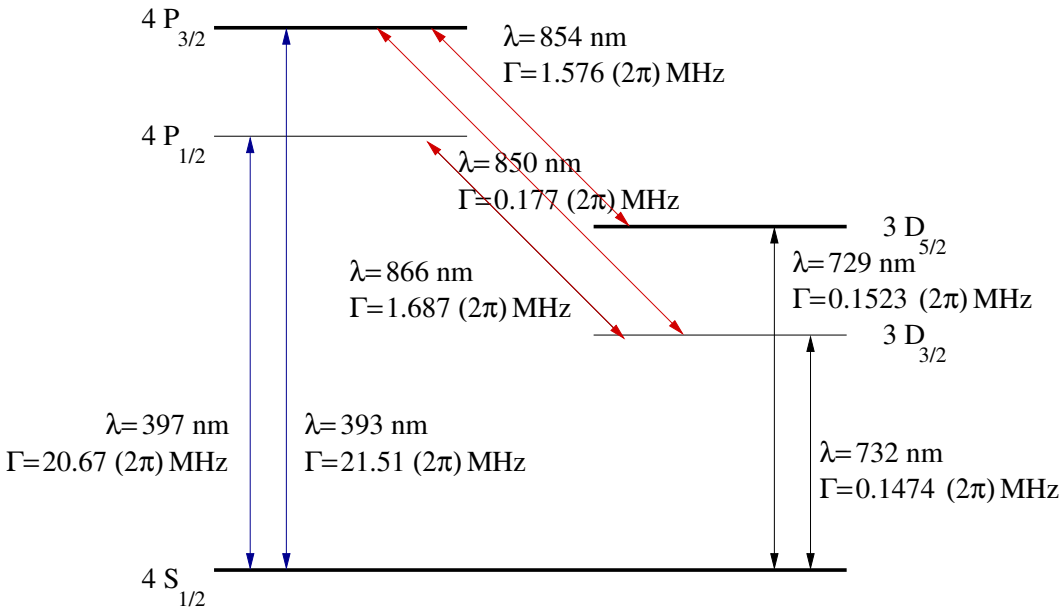

Figure 4.1: Levelscheme of $^{40}Ca^{+}$. The five lowest states of the ion are presented together with the transition wavelengths.

	λ_{air}	τ_{nat}	$\Gamma = 1/\tau_{\text{nat}}$
$S_{1/2} \leftrightarrow P_{1/2}$	396.847 nm	7.7(2) nsec	20.67 (2π) MHz
$S_{1/2} \leftrightarrow P_{3/2}$	393.366 nm	7.4(3) nsec	21.51 (2π) MHz
$S_{1/2} \leftrightarrow D_{3/2}$	732.389 nm	1.080 sec	0.1474 (2π) Hz
$S_{1/2} \leftrightarrow D_{5/2}$	729.147 nm	1.045 sec	0.1523 (2π) Hz
$P_{1/2} \leftrightarrow D_{3/2}$	866.214 nm	94.3 nsec	1.687 (2π) MHz
$P_{3/2} \leftrightarrow D_{3/2}$	849.802 nm	901 nsec	0.177 (2π) MHz
$P_{3/2} \leftrightarrow D_{5/2}$	854.209 nm	101 nsec	1.576 (2π) MHz

Table 4.1: Precise transition wavelengths of the lowest states in $^{40}Ca^{+}$, together with the natural lifetimes [18] .

The ratio of the spontaneous decay rates from the excited state $P_{3/2}$ to the ground state $S_{1/2}$ and the metastable state $D_{5/2}$ is 13.6:1. The equivalent ratio is to 12.2:1 for the decay of states $P_{1/2}$ to state $S_{1/2}$ and $D_{3/2}$.

Transitions between the S and D states are only allowed by quadrupol transitions with a transition rate of approximately (2π) 0.16 s^{-1}. This corresponds to the long lifetime of about 1 sec.

The goal is to reduce the level scheme of the trapped calcium to the desired three level $S_{1/2}$, $P_{3/2}$ and $D_{5/2}$. These states are chosen, as the other states will be used for measuring the atomic state. Without populating the $P_{3/2}$ state, red detuned light at 397 nm is used to initially cool the ion via the $S_{1/2} - P_{1/2}$ transition. As the $P_{1/2}$ and $P_{3/2}$ state might decay into the metastable $D_{3/2}$ state, additional laser light of 866 nm is used to pump population out of the state $D_{3/2}$. As it is shown in figure 4.1 on the facing page, one could also use laser light at 850 nm to pump population out of state $D_{3/2}$, but a laser at this wavelength is currently not available in the experimental setup. After this first cooling process, σ polarised light at 397 nm is used to pump as much population as possible into the $S_{1/2}, m_j = -1/2$, as this represent the absolute ground state of the system and will be used as the state to start the experiment with. Applying only light at the wavelengths 393 nm, 854 nm and 866 nm (to pump population out of state $D_{3/2}$), the wanted 3 level system is obtained.

The next step is to include the Zeeman splitting of the magnetic sub levels for an applied magnetic field in the experiment. Besides enabling the Zeeman sub levels, the magnetic field also defines the quantisation z-axis used for the experiment.

The Zeeman splitting is equal to:

$$\Delta E = g_j \mu_B B m_j \tag{4.1}$$

g_j is the Landè factor, B is the applied magnetic field, m_j the magnetic quantum number of the state and μ_B the Bohr magneton, defined

$$\mu_B = \frac{e\hbar}{2m_e} \tag{4.2}$$

Taking the magnetic field in units of Gauss, that is 10^{-4} Tesla, the Bohr magneton can be expressed in a frequency units as 1.39962 MHz $\approx$ 1.4 MHz.

The above mentioned Landè factor is described by the following formula [19]:

$$g_j = 1 + \frac{J(J+1) + S(S+1) - L(L+1)}{2J(J+1)} \tag{4.3}$$

The values for the 5 levels mentioned of the used calcium ion are presented in table 4.2 on the next page.

	$S_{1/2}$	$P_{1/2}$	$P_{3/2}$	$D_{3/2}$	$D_{5/2}$
g_j	2	2/3	4/3	4/5	6/5

Table 4.2: Landè factors for the 5 lowest levels of the $^{40}Ca^{+}$ ion

4.2 The ion trap

A linear Paul trap is used in the experiment to trap the $^{40}Ca^{+}$ ions. The basic idea came from Wolgang Paul in 1953, who suggested the mass selection of ions by a radiofrequency field [20].

The Paul trap can catch and hold charged particles of a certain mass-to-charge ratio [21], which is the reason for its widespread use in physics. Setting up such a trap in an ultra high vacuum (UHV), one is able to isolate the trapped ions from the environment and study the properties of single ions.

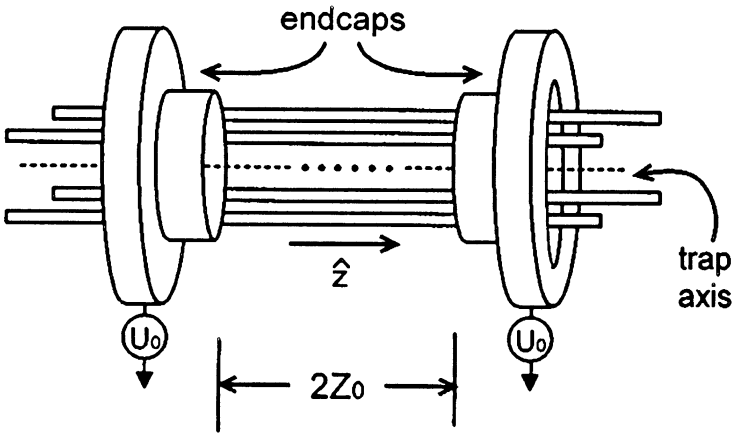

Figure 4.2: A quadrupole mass filter with endcaps forming an ion trap [22]. The four rods, connected to an appropriate RF source, confine ions of a certain range of charge-to-mass ratios in the radial direction. Additional endcaps at a positive potential (for positively charged ions) confine the ions in the axial direction.

A three-dimensional quadrupole field can be described by:

$$\phi(r) = \frac{\phi_0}{r^2} \sum_{i=1}^{3} \alpha_i x_i^2 \tag{4.4}$$

To fulfil Maxwell's equations, an electric potential in a vacuum must obey $\Delta\phi = 0$. This leads to the condition that $\sum_{i=1}^{3} \alpha_i = 0$, ruling out the possibility of trapping ions in a static field. Nevertheless an effective trap potential can be produced by applying an appropriate RF field. The layout of a linear Paul trap is shown in figure 4.2. Connecting one pair of diagonal electrodes to ground, while applying an ac-voltage of $V_0 \cos(\Omega t)$ to the other pair of diagonal electrodes, a trap potential

near the axis can be derived [22]:

$$V(x,y,t) = \frac{V_0}{2}(1 + \frac{x^2 - y^2}{R'^2})\cos(\Omega t) \tag{4.5}$$

R' would represent the perpendicular distance between the ideal hyperbolic cylinder rods and the trap axis. It will be approximated by R, the distance between the actual rods and the trap axis, as $R \approx R'$.

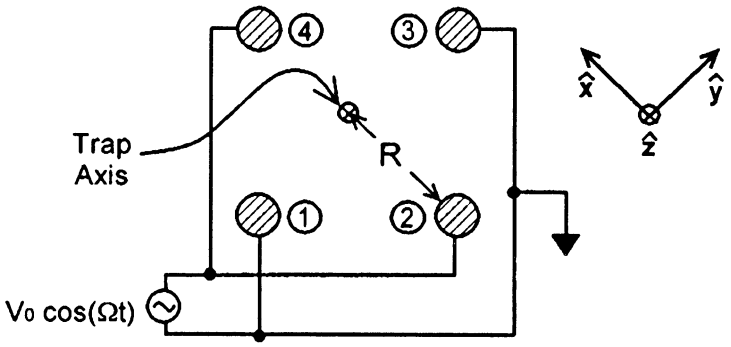

Figure 4.3: Electrical connections to the iontrap [22]

The gradient of the corresponding electric field confines the ion radially. To provide axial confinement, a potential U_0 is applied to the two endcaps, creating a static potential near the center of the trap:

$$U(x,y,z) = \frac{\kappa U_0}{Z_0^2}(z^2 - \frac{1}{2}(x^2 + y^2)) \tag{4.6}$$

with Z_0 equal to half the distance between the end caps and $\kappa(< 1)$ representing a geometrical form factor. At this point the small component of the alternating electrical field along the z axis due to the electrode configuration is neglected.

From equation 7.12 on page 74 and 4.6 the total electric field can be calculated to be:

$$E(x,y,z,t) = -V_0(\frac{x\vec{e}_x - y\vec{e}_y}{R'^2})\cos(\Omega t) - \frac{\kappa U_0}{Z_0^2}(2z\vec{e}_z - x\vec{e}_x - y\vec{e}_y) \tag{4.7}$$

Introducing the following substitutions:

$$a_x = a_y = -\frac{1}{2}a_z = -\frac{4Q\kappa U_0}{mZ_0^2\Omega_{rf}^2} \tag{4.8}$$

$$q_x = q_y = \frac{2QV_0}{mR'^2\Omega_{rf}^2},\ q_z = 0 \tag{4.9}$$

the equations of motion for a single ion of charge Q and mass m are equivalent to the Mathieu equation

$$\ddot{u}_i + (a_i + 2q_i\cos(\Omega t))\frac{\Omega^2}{4}u_i = 0 \tag{4.10}$$

where $\mathbf{u} = u_x\vec{e}_x + u_y\vec{e}_y + u_z\vec{e}_z$ is the position of the ion using the coordinate system shown in figure 4.3 on the previous page.

For $|q_i| \ll 1$ and $|a_i| \ll 1$ the solution of the Mathieu equation can be approximated by:

$$u_i(t) = u_{1i}\cos(\omega_i t + \phi_{Si})[1 + \frac{q_i}{2}\cos(\Omega t)] \tag{4.11}$$

with

$$\omega_i \simeq \frac{1}{2}\sqrt{a_i + \frac{1}{2}q_i^2} \tag{4.12}$$

while the constants u_{1i} and ϕ_{Si} are given by initial conditions.

Looking at the trajectories of the particle, two movements can be distinguished: A secular motion that is a harmonic oscillation with frequency ω_i, superposed by a micromotion. This micromotion oscillates with the frequency of the applied RF signal. The farther the particle moves away from the center of the trap, the bigger this oscillation becomes.

Neglecting the amplitude of the micromotion, the secular motion is interpretated as a harmonic motion, that is caused by an effective harmonic potential:

$$\Phi_{\text{eff}} = \frac{1}{2}\sum_{i=1}^{3} m\omega_i^2 x_i^2 \tag{4.13}$$

As the atoms, ejected by the oven, normally have energies of a few 35 meV up to about 100 meV, they can be easily trapped since the parameters of the trap are chosen to result in trap depths of some eV.

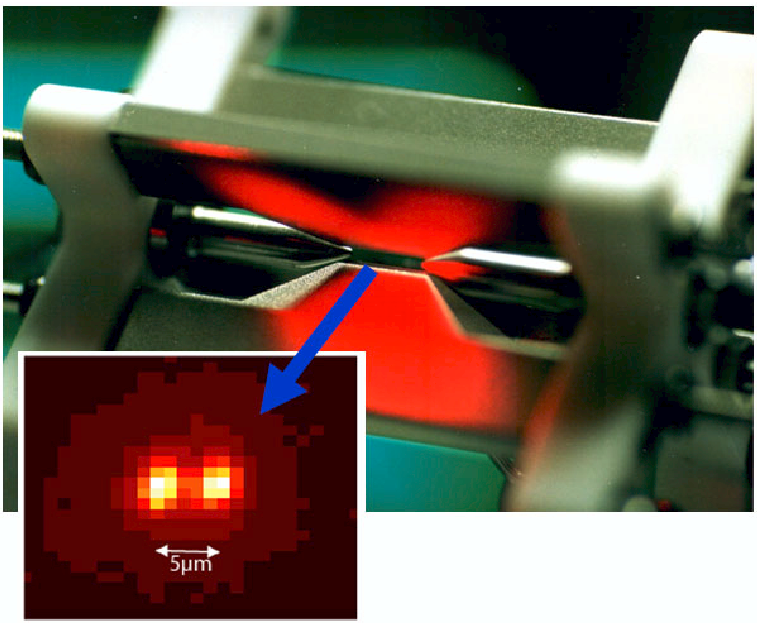

Figure 4.4: The ion trap used in Innsbruck, and an image of stored ions

4.2.1 Laser cooling of trapped ions

The trapped ions are held in a harmonic potential. Nevertheless the ions, and especially an initially loaded ion cloud, can be considered "hot". A possibility to cool the motion of the trapped ions was suggested first in 1975 by Haensch and Schawlow for free atoms [23] and by Wineland and Dehmelt for trapped ions [24].

Slightly red-detuned laser light is shone on the ions. Whenever the atoms move towards the light source with an appropriate velocity, the atoms are able to absorb a photon. This involves a momentum change equal to $-\hbar k$ due to the photon. This momentum represents a deceleration of the atom. As the emitted photons are radiated in any direction, multiple emissions results in no effective momentum change. The atom is effectively slowed down in the direction of the red-detuned light source. Using several beams to shine at the atom from all directions, the motion can be reduced in all directions, resulting in a cooling of the atom.

The same theory can be applied to trapped ions, with the small difference that the trap potential has to be included in the theory. As long as the lifetime of the excited state is much shorter than the period of the secular motion, meaning that the ion doesn't change position or momentum during an emission/absorption, the trapped ion can be regarded as similar to a free atom. The only difference is, that, in theory, one beam is sufficient to cool trapped ions in all directions, as long as it projects on all directions of motion.

The minimum energy that can be achieved through this procedure is [25]:

$$E_{\min} = \frac{\hbar\Gamma}{2} \tag{4.14}$$

and is dependent on the linewidth of the cooling transition.

This allows one to cool the ions, under certain circumstances, to the "Lamb-Dicke regime", that is, the spatial uncertainty of the atom becomes smaller than the wavelength of the atomic transition.

Another, additional, method to cool the ions, is sideband cooling. Since the potential that traps the ions is described by a harmonic potential, the states of motion can be thought of as the excited states of a quantum oscillator. These are seen as sidebands on the on the atomic transition, separated by the trap frequency on the excitation spectrum of the ion. These sidebands can only be resolved, if the natural linewidth of the transition is smaller than the trap frequency. This is called 'strong confinement'.

The principle behind sideband cooling is shown in Figure 4.5 on the following page. The harmonic trap potential represents quantised states of motion, called phonons. These are dressed with the two-level system of the trapped ion. Together, they represent a level scheme, that allows transitions from different states of motion (different phonon numbers) via a change in the electronic excitation. Using a laser

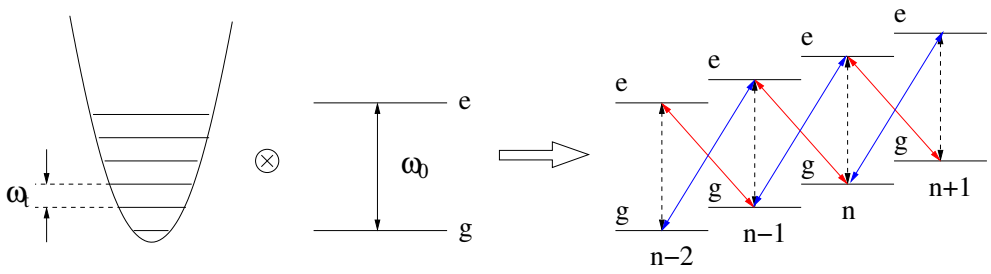

Figure 4.5: Sideband cooling: The atomic ground and excited state are dressed with the harmonic oscillator states. Detuning from the atomic transition (carrier, drawn in black) allows either motional cooling (red-detuned, indicated by red transitions) or heating (blue-detuned, displayed as blue transitions).

resonant with the red sideband, a motionaley excited ion in the electric ground state can be transferred into a lower state of motion, that is electronically excited. The excited state can decay to the electric ground state, allowing further cooling of the motion. The possibility to change the index of motion is crucial for sideband cooling and can be described by [25]:

$$W_{n\to n'} = |\langle n|e^{-ikr}|n'\rangle|^2 \simeq \delta_{nn'} + \eta^2(n'\delta_{n,n'-1} + (n'+1)\delta_{n,n'+1}) + \dots \tag{4.15}$$

As can be seen from this equation, the probability to get from phonon number n' to n via a momentum transfer is calculated and expressed in terms of η. δ represents the Kronecker-Delta, depending on the phonon number.

ν is known as the Lamb-Dicke parameter, and is equal to:

$$\eta^2 = \frac{\epsilon}{\omega} = \left(\frac{\pi a_0}{\lambda}\right)^2 \ll 1 \tag{4.16}$$

where $\epsilon = \hbar k^2/2m$ is the change of energy due to photon emission or absorption, and a_0 is the spatial extent of the groundstate in the harmonic potential, equal to $\sqrt{\frac{\hbar}{2\omega_i m}}$. This can be calculated by:

$$\langle x_i\rangle = \langle n|x_i|n\rangle = 0 \tag{4.17}$$

$$\Delta x_i = \sqrt{\langle n|x_i^2|n\rangle - \langle n|x_i|n\rangle^2} = \sqrt{(2n+1)\frac{\hbar}{2\omega_i m}} \tag{4.18}$$

It relates the uncertainty in the ions position to the wavelength of the light. For the limit $\eta \ll 1$, i.e. the Lamb-Dicke regime, only neighbouring motional states can couple to one another, as higher terms in equation 4.15 will be neglected. Changes in the index of motion by ± 1, from an initial index of n, are suppressed by a factor of $n\eta^2$.

The smallest index of motion that can be achieved by sideband cooling in the Lamb-Dicke regime is given in the strong coupling regime $\gamma \ll \omega_t = \Delta$:

$$\langle n\rangle = \left(\frac{\gamma}{\omega_t}\right)^2 \left(\alpha + \frac{1}{4}\right) \tag{4.19}$$

where α depends on the transition used for cooling. For a dipole radiation pattern it is equal to 2/5 (for more details, see ref. [25]). For a small linewidth, this value can be approximately zero, representing a high probability ($> 90\%$) to find the ion in the motional ground state.

4.3 The optical resonator

The optical resonator will replace one of the lasers mentioned in the theory given in Chapter 2 and Chapter 3. In order to achieve a high electric field that allows a good coupling between the resonator and the atom, the smallest possible mode volume has to be achieved. The following will explain the used terms and gives an overview of the important properties for the experiment.

An optical resonator is most simply built from two mirrors, reflecting the light back and forth. By reflecting the light as many times as possible between the two mirrors before it leaks out of the cavity, the light field can be highly enhanced.

A measure for this is the finesse of the resonator, defined as π times the average number of photon traversals in the cavity before leakage through a mirror. This can also be understood as an energy storage time τ, depending on the finesse of the cavity:

$$F = \frac{\pi c}{L}\tau \tag{4.20}$$

where τ is the time constant of the intensity decay of an optical resonator. Another convenient parameter is the decay rate of the electrical field, κ:

$$\kappa = \frac{1}{2\tau} = \frac{c\pi}{2FL} \tag{4.21}$$

The finesse can also be defined by the spectral width of the modes of the cavity:

$$F = \frac{\nu_f}{\delta\nu} \tag{4.22}$$

where ν_f is given by:

$$\nu_f = \frac{c}{2L} \tag{4.23}$$

ν_f is the 'free spectral range', while $\delta\nu$ is the FWHM of the transmission peak.

Neglecting absorption losses and assuming geometrically perfect substrates, the finesse of the resonator depends only on the reflectivity of the two mirrors and is given by [26]:

$$F = \frac{\pi\sqrt{r_1 r_2}}{1 - r_1 r_2} \simeq \frac{\pi}{1 - r_1 r_2} \tag{4.24}$$

While a high finesse is important, the light of the resonator should also be focused tightly on the ion, requiring a small mode volume, approximated with $L\pi\omega_0^2$, and a small beam waist.

For a symmetric cavity of length L, and mirrors with a radius of curvature of R, the waist size of the TEM_{00} mode at the center of the cavity is given by [26]:

$$\omega_0^2 = \frac{\lambda}{2\pi}\sqrt{L(2R-L)} \tag{4.25}$$

For a fixed L, the resonator with the smallest waist size is a near-concentric resonator, consisting of two mirrors with a radius of curvature only sightly larger than half of the distance between the mirrors (see fig. 4.6).

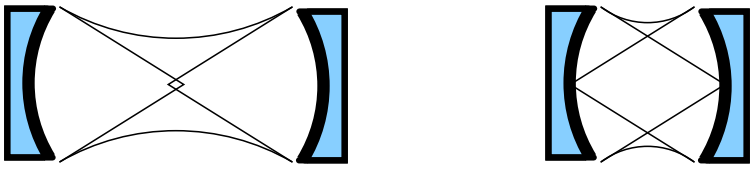

Figure 4.6: Different setups of optical resonators. To the left, a nearly concentric cavity is shown. It has the smallest beam-waist at the center, compared to other cavity layouts. To the right, a confocal cavity is shown. The name results from the fact that the focal length of the mirrors is twice their radius of curvature. Therefore, mirrors with a distance between them that is equal to their curvature, should have their foci at the same point.

For $R = (L + \Delta L)/2$, equation 4.25 can be rewritten as:

$$\omega_0^2 = \frac{\lambda}{2\pi}\sqrt{L\Delta L} = \frac{L\lambda}{\pi}\sqrt{\frac{\Delta L}{4L}} \tag{4.26}$$

As a near-concentric cavity results in a very narrow waist, the spot size is very large at the mirrors (see figure 4.7 on the facing page):

$$\omega_{mirr}^2 = \frac{L\lambda}{\pi}\sqrt{\frac{4L}{\Delta L}} \tag{4.27}$$

Therefore sufficiently large mirrors must be used, while still allowing a good optical access to the ions.

Another practical problem of a near concentric setup is the alignment of the optical axis of the mirrors. As shown in Figure 4.8 on the next page, even slightest alignment errors will tilt the cavity mode by an angle θ, that can be approximated by:

$$\theta \approx \tan(\theta) = \frac{\Delta x}{\Delta L} \tag{4.28}$$

where Δx represents the horizontal deviation of the focus of one mirror from the optical axis. This may easily result in a mode hitting the edge of the high-reflection coated mirrors and therefore lead to increased losses.

The mode volume could be reduced further by minimising the scale of the whole resonator setup. The minimum distance in our experiment is already set by the size of the trap, as the resonator must be installed around the trap.

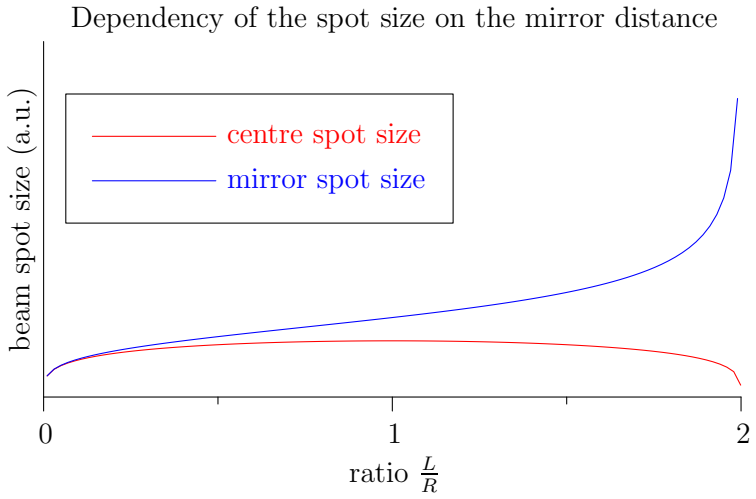

Figure 4.7: Beam spot size at the center and mirrors of a cavity mode, depending on the ratio of mirror distance L and radius of curvature R.

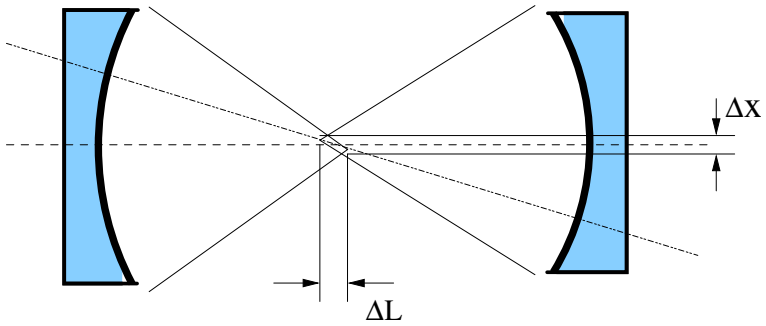

Figure 4.8: Problems with a near convocal resonator: A very small tilt of the mirrors will, due to the near critical setup of the mirror distance, immediatly result in a large alteration of the optical axis.

As was discussed in Chapter 2, the coupling between the field and the atom depends on the dipole transition element times the electric field. The question arises, whether a field is present in an empty cavity. The value of the electric field can be obtained by setting the electromagnetic energy $\varepsilon\mathcal{E}_0^2 V$ equal to the energy of half a photon: $\hbar\omega/2$ [27]. This idea comes from theoretical thoughts during quantising a light field with a sum of harmonic oscillators. A harmonic oscillator in the ground state still yields an energy equal to half it's excitation energy. Using this residual energy, the field can then be described by:

$$\mathcal{E}_0 = \sqrt{\frac{\hbar\omega}{2\varepsilon_0 V}} \tag{4.29}$$

The mode volume is equal to

$$V = \frac{\pi L \omega_0^2}{4} \tag{4.30}$$

Reducing this parameter will lead to a very high coupling energy $\hbar g = |D.\mathcal{E}_0|$ between the field of the cavity $\mathcal{E}_0$ and the dipole of the atom D.

Finally the coupling strength g has to be calculated. As g is given by the interaction Hamiltonian, and the field of an empty cavity is already known, only the dipole elements need to be calculated.

$$g = \frac{e\mathcal{E}_0}{\hbar}\langle g|r.\epsilon|e\rangle \tag{4.31}$$

The matrix element $\langle g|r.\epsilon|e\rangle$ can be calculated by the Wigner-Eckhart theorem [18]:

$$\langle g|r.\epsilon|e\rangle = \sqrt{\frac{A}{c\alpha k^3}}\sigma \tag{4.32}$$

$$\sigma = \sqrt{\frac{3(2j'+1)}{4}}\left|\sum_{q=-1}^{1}\begin{pmatrix} j & 1 & j' \\ -m_j & q & m_j' \end{pmatrix} c^{(q)}\epsilon^{(q)}\right| \tag{4.33}$$

k represents the wave vector $k = 2\pi/\lambda$, α the fine structure constant, $\alpha = e^2/4\pi\epsilon_0\hbar c \approx 1/137$. $A = 2\gamma$ is the Einstein coefficient of the transition. σ is a scale for the strength of the coupling and includes the Wigner 3-j symbol, that can be calculated as shown in [28]. The polarisation of the light is taken care of by $p^{(q)} = c^{(q)}\epsilon^{(q)}$. Assuming that the polarisation of the light is chosen to optimally perform the transition, represented by setting $p^{(q)} = 1$, σ may be calculated for the different Zeeman components of the $P_{3/2} - D_{5/2}$ transition. The results are presented in table 4.3 on the facing page.

Using these equations and results, the final coupling strength g of the transition $|P_{3/2}, m_j = -3/2\rangle - |D_{5/2}, m_j = -5/2\rangle$ with the field of an empty cavity can be calculated to be:

$$g = \sqrt{\frac{2c\gamma\lambda^2}{\pi^2 L\omega_0^2}} \tag{4.34}$$

$D_{5/2}$ $P_{3/2}$	-3/2	-1/2	1/2	3/2
-5/2	$\sqrt{\frac{1}{2}}$	0	0	0
-3/2	$\sqrt{\frac{1}{5}}$	$\sqrt{\frac{3}{10}}$	0	0
-1/2	$\sqrt{\frac{1}{20}}$	$\sqrt{\frac{3}{10}}$	$\sqrt{\frac{3}{40}}$	0
1/2	0	$\sqrt{\frac{3}{40}}$	$\sqrt{\frac{3}{10}}$	$\sqrt{\frac{1}{20}}$
3/2	0	0	$\sqrt{\frac{3}{10}}$	$\sqrt{\frac{1}{5}}$
5/2	0	0	0	$\sqrt{\frac{1}{2}}$

Table 4.3: Coupling σ between the Zeeman components of the $P_{3/2} - D_{5/2}$ transition

The relevant scale for a large coupling is set by the rate of other dissipative processes in the system. These are spontaneous emission of the atom by transitions that do not couple to the cavity, $\gamma_{\mathrm{non-trans}}$, like a $P_{3/2} - S_{1/2}$ decay, and leaking of photons out of the cavity, κ.

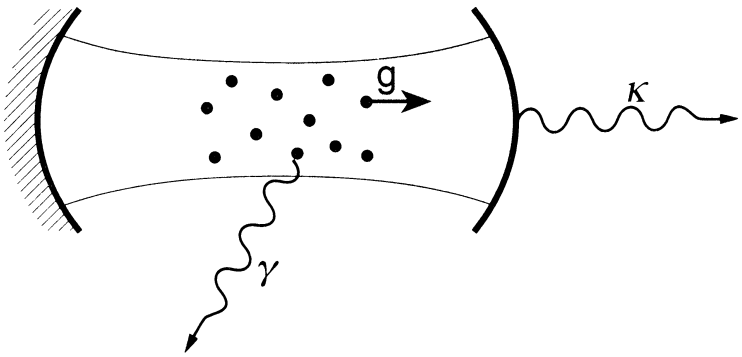

Figure 4.9: Reduced system parameters for cavity coupled atoms (taken from [29]). After all considerations, the whole system of interaction can be reduced to g, the coupling strength of cavity–atom interaction, $\gamma_{\mathrm{non-trans}}$, representing decays that do not couple to the cavity mode, and κ, the photon decay out of the cavity.

There are two interesting regimes: a strong and a weak coupling regime. In the strong coupling regime, $g \gg \kappa$ and $g \gg \gamma_{\mathrm{non-trans}}$, the photon will stay in the cavity for a very long time compared to the timescale of dissipative processes. This allows the realisation of Rabi oscillations with a single photon in the cavity. Although this is an interesting possibility, it does not allow the realisation of the desired stationary–flying qubit transformation.

In order to get the photon out of the cavity and send it to another quantum system, the "bad cavity regime" within the weak coupling regime defines the desired parameter space. Therefore, the following conditions have to be met:

All the theory presented so far was derived from an idealised model where the photon produced during a state transfer couples to the cavity, representing a one dimensional simplification. Clearly the atom can emit a photon in any direction. A

	Condition
Strong coupling:	$g \gg \kappa$ and $g \gg \gamma_{\text{non-trans}}$
Weak coupling:	$4g^2 < (\gamma_{\text{non-trans}} - \kappa)^2$
bad cavity regime	$\gamma_{\text{non-trans}} \ll g^2/\kappa \ll \kappa$
bad atom regime	$\kappa \ll g^2/\gamma_{\text{non-trans}} \ll \gamma_{\text{non-trans}}$

Table 4.4: Conditions for the different regimes of cavity–atom interaction

relevant parameter to describe the enhanced possibility of emitting the photon into the cavity mode is given by the cooperativity C, defined by [29]:

$$C = \frac{g^2}{2\gamma_{\text{non-trans}}\kappa} \tag{4.35}$$

This parameter is also related to the fractional emission into the cavity [30], β:

$$\beta = \frac{2C}{2C+1} \tag{4.36}$$

The cavity surrounding the trapped ion also changes the decay characteristics of the ion. The interaction with the cavity leads to a stronger transition between the used states $P_{3/2} - D_{5/2}$ via photon emission into the cavity. Decay by emitting light of other wavelengths is suppressed. The enhancement is described by the Purcell factor [31] and can be calculated by the cooperativity:

$$\bar{F} = 2C + 1 \tag{4.37}$$

The decay rate in the resonator is enhanced by this factor according to:

$$\gamma' = \gamma\bar{F} \tag{4.38}$$

where γ is given by the spontaneous decay of the transition in the vacuum field.

Although the validity of the substitution in the Raman passage of a laser by a cavity may not be readily apparent, a high finesse and a small mode volume allow this exchange with the large electric field of a laser beam. Especially looking at the presented theory, the analogy is given by explaining the correlation of Ω, that was used to describe the coupling of a laser, to g. The only difference is the number of photons in the field. Nevertheless, high fields can be achieved by tuning the available mode volume, allowing a rather strong coupling between the atom and the field, with an additional high probability of emitting the photon into the cavity mode.

4.4 The compound system

The experimental setup was designed and built by Carlos Russo. A schematic of the trap, the cavity and laser beams is shown in Figure 4.10 on the next page.

Light of a wavelength of 785 nm is used to stabilise the length of the cavity via a Pound–Drever–Hall lock[32]. This light is far away from any transition of the calcium ions and can, to a large extent, be ignored as a possible influence on the ions.

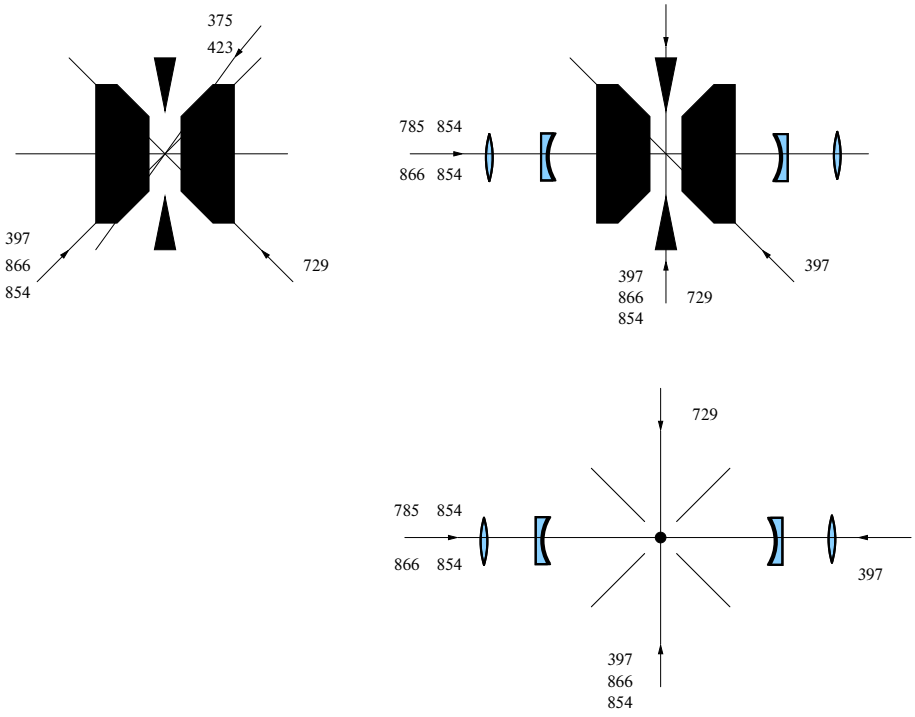

Figure 4.10: Lasers passing through our setup: The bottom right explains the beam paths if the observer looks at the experimental setup from above. Top right shows the beam trajectories with the observer standing in front of the setup, while top left explains the optical setup if regarded from the right hand side

After applying light of wavelengths 397 nm and 866 nm, the ions are prepared in the ground state $S_{1/2}, m_j = -1/2$ by a σ polarised beam of 397 nm. The first experiments that can be done are investigations of population transfer from $S_{1/2}$ to $D_{5/2}$ by using the laser at wavelength 393 nm, offset from resonance by an array of acousto-optical modulators, and a frequency–offset–locked laser at 854 nm.

Following these first experiments, the cavity will be locked to the wavelength of the 854 nm laser system with the 785 nm laser, in order to replace it in the experiment of population transfer. Then the 854 nm laser will be turned off. In other words, the 854 nm laser is only used as an initial frequency reference, indicating the correct cavity resonance.

Piezo crystals allow movement of the whole cavity assembly with respect to the position of the trap. As the ions are confined in a very small volume, this is a crucial control for the experiment. Mundt [33] has shown a dependence of the excitation probability on the ion's position in the standing wave. The obtained data are shown

in figure 4.11.

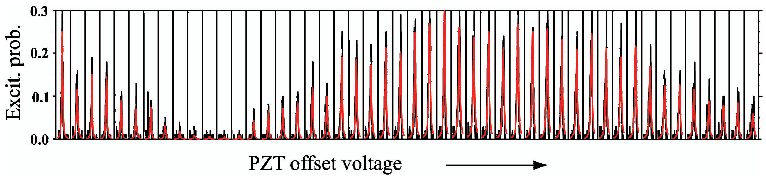

Figure 4.11: An offset voltage was applied to a piezo pair to move a cavity around a trapped ion, allowing the investigation of the excitation probability depending on the position of the ion in the cavity [33].

Once these optimisations have been done, further investigation of this quantum system consisting of single ions, single photons and their interaction, may be performed.

Future milestones include the following:

- Doppler cooling of a single trapped ion
- state preparation via a σ beam of 397 nm
- test of a population transfer with 393 nm and 854 nm, both with an offset to the atomic transitions
- locking of the cavity to the wavelength of the 854 nm laser
- state preparation and population transfer with the cavity as 854 nm replacement

Once this state transfer is done, further research on single photon production can be performed.

Chapter 5

Frequency offset lock

As explained in chapter 3, to coherently move a population using a Raman pulse from one state to another in the presence of spontaneous emission, the lasers must be detuned from the transition. This detuning reduces the probability of spontaneous emission from the intermediate level. To achieve a stable and well-defined offset, it is necessary to lock the Raman laser with such an offset to a resonant laser.

In order to lock a laser system to a certain frequency offset, an error signal must be derived, which corresponds to the deviation between desired frequency offset and actual frequency difference between the two lasers. Using appropriate servo systems, this error signal is used to stabilise the laser to the desired frequency offset.

Different approaches of error signal generation for a frequency offset lock are presented and their properties discussed. This will be followed by an introduction to possible servo systems for controlling the wavelength of emitted laser light, allowing the closure of the locking loop.

5.1 Schemes

There are many different approaches known to realise a frequency offset lock between two lasers, but not all of them can be applied to the given setup for different reasons.

One scheme for creating a frequency offset is the use of an array of acousto-optical modulators (AOMs). Each AOM shifts the first order diffracted beam by the applied RF frequency. Building an array of AOMs with different operating frequencies, one can obtain almost any desired frequency offset. One drawback of this scheme is the diffraction efficiency less than unity. Another one is the low bandwidth of the AOMs. One can not cover frequency ranges of more then 400 MHz with one AOM, resulting in the necessity of tuning several AOMs of the array in order to perform the desired frequency offset of about 100 MHz up to 1 GHz. Additionally it's a more expensive solution, as the cost of AOMs is rather high.

A passive frequency lock with optical feedback can be realised by injection locking. The principle of this locking scheme is to inject a low noise, low power laser into a high power laser. The increased gain in the mode corresponding to the injected laser frequency causes the high power laser to preferentially lase with the same frequency as the low noise laser. The scheme can be applied to establish a frequency-offset lock. As presented in [34], one can introduce frequency sidebands on the low noise source via an electro-optical modulator (EOM). Using a Fabry-Perot cavity as an optical bandpass filter, one can filter one sideband of the emitted light. Injecting this light into the high power laser, one establishes a frequency-offset lock between the carrier of the low noise laser and the injection locked laser with an offset frequency equal to the RF driving frequency of the EOM. The problem with this approach is the amount of technical effort that is needed to stabilise the Fabry-Perot cavity and tune it in tandem with the offset frequency.

A similar setup was presented by Clarke in 1998 [35]. A master laser's current is modulated. By injecting a low noise light source, the slave laser can be locked to one of the resulting sidebands. Although this approach is simpler, laser light of the carrier frequency is also emitted to some extent. As our Raman experiment depends on a pure S-D transition without populating the spontaneously decaying P state, this scheme is unsuitable.

Therefore, in the following, only schemes that produce a single laser light frequency at the output of the locked laser will be considered. This may easily be done by using electrical feedback. The basic setup normally consists of two lasers and a photodiode (PD). One laser, which is called the master laser, emits light at a wavelength equal to the employed atomic transition and will be used as reference frequency. The second laser, called the slave, will be controlled in such a way, that it has a fixed frequency offset from the master. The first stage in doing this is to produce a beat signal of those two lasers on the photodiode. The beat signal, equal to the frequency difference between the two lasers, is then used to obtain an error signal for the offset lock.

The signal of the photodiode is connected to a circuit which produces an error signal. The error signal is an output voltage, which is positive if the beat frequency is higher then the desired offset frequency, or negative for a lower frequency. By feeding this voltage into the laser control of the slave laser, one is able to set the laser frequency to a fixed offset compared to the master.

Most circuit layouts determine only whether the input frequency is higher or lower than a hard-wired lock frequency, and allow no tuning of the offset. To work with a different offset frequency than this default, the beat frequency $\Delta\nu$ (representing the frequency difference between the two lasers) is normally mixed-down to the hard-wired lock frequency via a local oscillator at frequency ν_{vco} (see figure

5.1). The advantage is that one can lock to any frequency as long as one is able to provide the right frequency at the local oscillator and a mixer that is able to handle the relevant frequencies. Now that one has the (mixed-down) beat signal, there are several ways to produce an error signal for the servo system of the slave laser.

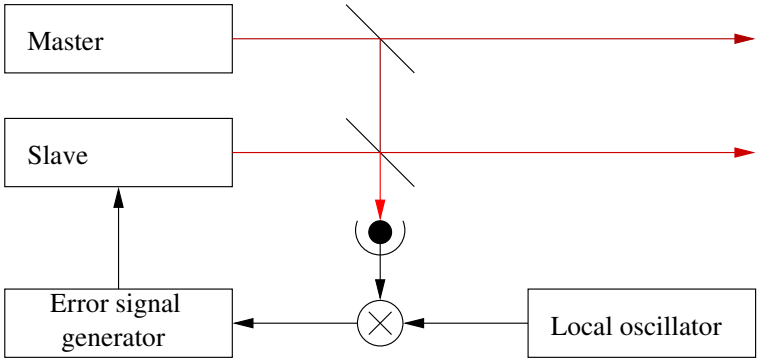

Figure 5.1: Basic setup of an optical laser frequency offset. The beat signal of two light sources is observed on a photodiode. Depending on the error signal generator, this beat signal might be mixed to a certain frequency range via a mixer and a local oscillator.

On the following pages, three approaches to producing a suitable error signal will be discussed in more detail. The first one employs a chip that directly converts a frequency input to a DC voltage. Secondly, a method using a delay line to produce an error signal via a phase detector is presented. Finally, a scheme using a high-pass filter as a frequency-to-power converter is presented. Advantages and disadvantages of the presented approaches will be discussed.

5.1.1 Frequency-to-voltage converters

The ideal solution would be to use a single chip which takes a frequency as an input, and directly outputs a voltage according to the frequency applied. Using a commercial frequency-to-voltage converter it is easy to obtain such an error signal. Most converters require TTL pulses at the input. Therefore the beat signal from the photodiode (PD) has to be converted into TTL pulses by a comparator. One of the limitations of frequency-to-voltage converters is that they often have a very narrow bandwidth and operational frequency range. Therefore the signal, in addition, has first to be divided to an appropriate frequency range.

In this, as with the following schemes, one obtains an output voltage that depends on the applied input frequency. To obtain an error signal that can be used to stabilise the laser via a servo system (assuming that the servo tries to lock to an error signal that is zero), one would have to change this signal in such a way, that the signal of the circuit is zero at the desired offset frequency. This is easily done by measuring the output voltage of the chip, looking up to voltage that corresponds

to the desired lock frequency, and subtracting it from the chip output voltage. This results in an error signal, that is zero if the input frequency equals the desired lock frequency, and is either positive or negative for other frequencies. A schematic setup of this scheme is shown in figure 5.2.

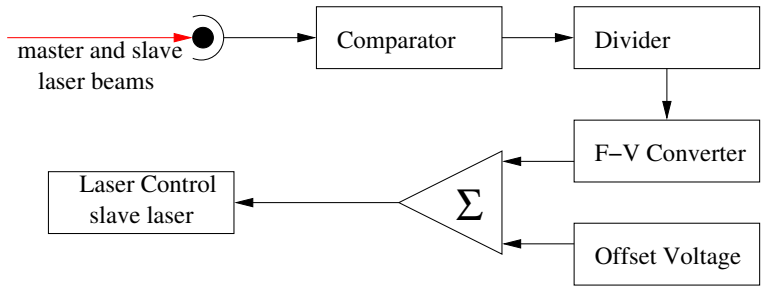

Figure 5.2: Example of an offset lock using a frequency to voltage converter. A comparator produces TTL pulses, that are divided to a frequency in the operating range of the frequency–to–voltage converter. Adding an offset, an error signal is derived.

The advantage of this setup is its simplicity and stability. As reported in [36], a relative frequency deviation of the lasers below 400 Hz for a time span between 0.1 s and 8000 s is achievable. The limiting factors are the finite gain of the setup and especially the drifts of the output voltage of the frequency to voltage converter. Also, this scheme strongly depends on stable dividers. Since the converters normally only have very limited bandwidth and frequency range, the dividers play a crucial role in this setup.

5.1.2 Locking with a delay line

Another simple scheme was proposed by H.N. Rutt in 1984 [37]. The idea behind this scheme is to split the mixed-down beat signal ($\Delta\nu - \nu_{\mathrm{vco}}$), to delay one part by a constant time (independent of the frequency), and mix the signals again on a phase detector. A low-pass filter will suppress the signal of the doubled frequency. The output is a DC signal, whose level will vary sinusoidally with the delay time or with the frequency difference.

In equation 5.1, $\Delta\nu$ corresponds to the beat frequency, ν_{vco} to the frequency of the local oscillator (as previously introduced) and τ represents the induced time delay.

$$V_{\mathrm{err}} \propto \cos(2\pi(\Delta\nu - \nu_{\mathrm{vco}})\tau) \tag{5.1}$$

Depending on the desired specifications, one can either choose a long delay line to produce a steep slope, resulting in a tight lock, or use a shorter time delay which produces a greater capture range. Assuming that the time delay of a BNC cable is independent of the frequency, τ can easily be adjusted by choosing a proper length of a BNC cable. This allows an easy and fast access to this parameter of the lock.

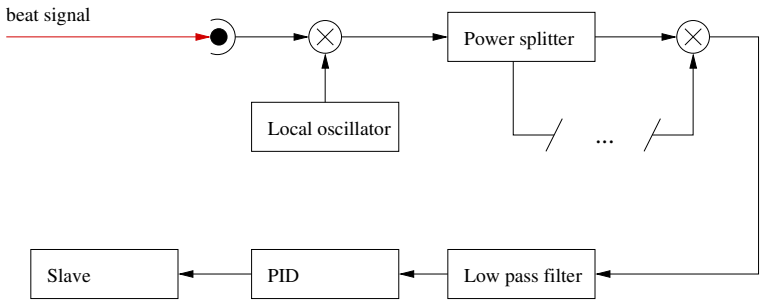

Figure 5.3: Offset lock using a delay line. Introducing a time delay with a BNC cable, this delay can be used to generate an error signal at a phase detector.

Recently this scheme for building a frequency offset lock was used by Schuenemann et al [38], showing the expected error signal with its multiple locking points and an envelope resulting from the limited bandwidth of the phase detector (see Figure 5.4).

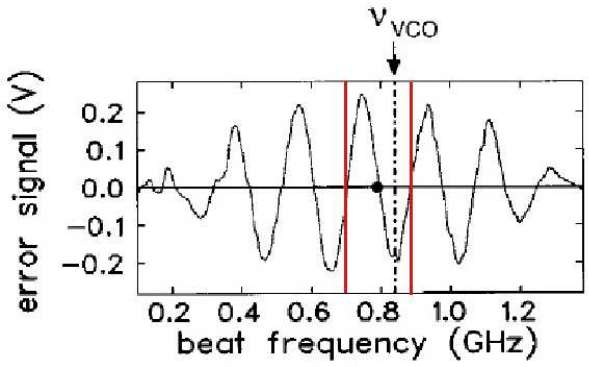

Figure 5.4: Measured error signal of a delay line setup. The dot indicates one of the locking points. ν_{VCO} denotes the frequency of the RF signal that was used to shift the beat signal. The red bars have been added to the original graph in order to better visualise the capture range of about ±100 MHz as well as a linear slope around the lock frequency. Taken from [38]

Using an ordinary BNC cable, they introduce a frequency independent time delay of 5 ns per meter, equivalent to a distance between the different locking points of 200 MHz. The capture range is roughly half the separation of the adjacent lock points, i.e. ±100 MHz, which should be sufficient to recover from all frequency jumps that normally occur in a laboratory.

A disadvantage of the scheme is that there are multiple lockpoints. In addition, there is no way to independently adjust the capture range and the steepness of the error signal. There is always a compromise between those two important parameters.

5.1.3 A high-pass filter as a frequency-to-voltage converter

Another technique was recently published by Ritt [39]. A high-pass filter on its own represents a 'frequency-to-power' converter. By adding basic electronic elements, the power can be converted into a voltage, resulting in a simple circuit layout that produces an error signal whose slope depends only on the chosen filter.

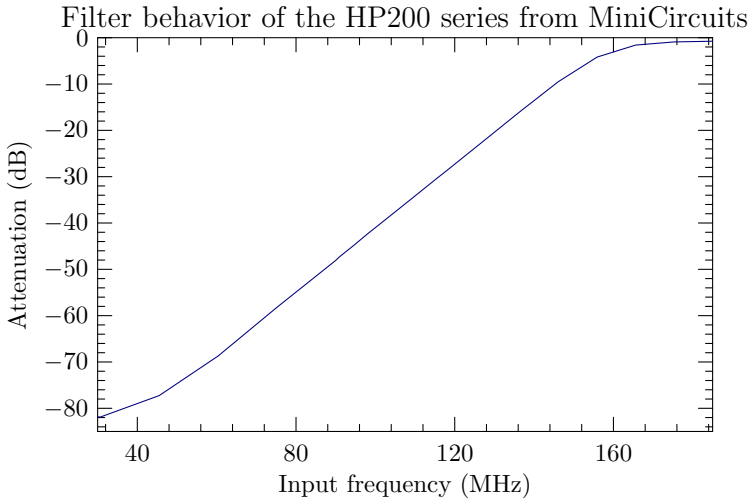

Figure 5.5: Frequency response of a high-pass (MiniCircuits PHP200)

From figure 5.5, the basic concept is easy to understand: assuming a constant input power, one can compare the output power of the filter with the response curve from its datasheet. Using the output power at the desired frequency offset as a set-power, one only needs to add a circuit that gives an output voltage proportional to the difference between the output power and the set-power.

An obvious advantage is that there is only one lockpoint, as a given attenuation of the filter corresponds to only one input frequency. In addition, as can be seen from the sample in figure 5.5, a very large capture range is obtained. The range is limited to the lower side by the lock frequency itself, and is limited for positive frequency jumps only by the possibility of the diodes to rectify the signal. This corresponds to frequencies much higher than 500 MHz.

The complete circuit that produces the error signal is shown in figure 5.6 on the facing page. An applied input signal is split into two parts. The first part passes through a high-pass filter and is attenuated according to its frequency. Using a diode and a low pass filter, this power is transformed into a positive DC-voltage. The reason for this is the diode, that rectifies the signal. The capacitor of the low-pass filter is charged during one phase of the signal and discharges during the other, effectively smoothing the output. Together, the output signal can be regarded as a DC signal, with a small oscillation on it, depending on the cutoff frequency of the low-pass filter. The second part of the input signal is transformed by same

means into a negative DC-signal (with the diode set in the opposite direction). These two voltages are then added together. The desired lock frequency is given by the difference between the additional attenuation in the two paths. The set point is the frequency at which the attenuation of the high-pass filter is equal to the difference between the two fixed attenuators. If the input frequency is below the lock frequency, the power will be attenuated more in the high-pass path, resulting in a smaller positive voltage, leading to a negative voltage at the output. For frequencies higher than the lock frequency, more power will be transformed into a higher positive DC-voltage, resulting in a positive output voltage.

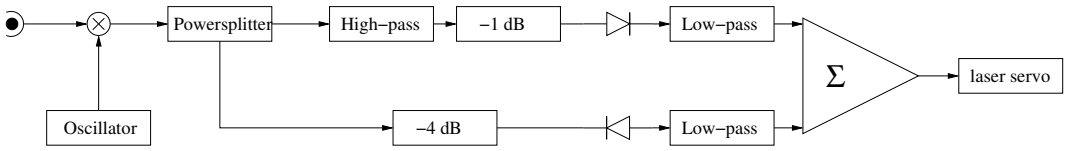

Figure 5.6: Error-signal producing circuit using a high-pass filter. The mixed down signal is split into two arms. In one of them, the high-pass filter introduces the frequency dependence of the circuit. A diode with a low-pass filter is then used to convert the different power levels into voltages.

An important criterion for the usefulness of an offset lock error signal generator is the steepness of slope at the lock frequency. In this case it is given by the steepness of the slope of the high-pass filter. Since a high-pass filter is a very basic and simple device, and can easily be built according to desired properties, this component can be tuned to have almost any desired steepness. Overshoots and other normally undesirable behaviour of filters can be neglected, as they are far from the lock point. In this region just the sign of the error signal is important and deviations from the ideal behaviour won't have any influence on the tightness of the lock.

Another important criterion of the circuit is the bandwidth. As the lock will be running at a certain RF frequency, we shall refer to the bandwidth as an operational bandwidth. It is limited by the low-pass filters that are used to produce the DC-signal. These low-pass filters can be chosen to result in a rather high bandwidth for the circuit as the lock frequency will be set to be above 100 MHz. RF-sources in the laboratory typically work at 20 MHz and higher. Therefore these low-pass filters may have a cut-off frequency of about 5 MHz without risking signal pick-up from other RF-sources nor losing precision of the error signal, as the lock point is set to a far higher frequency.

The steep slope and large bandwidth are the reasons that make this scheme superior to the other schemes presented. Not only does one have easy access to important parameters of the circuit, like steepness of the slope at the lock-frequency and the operational bandwidth, but one is also able to set them independently to

values that are hard to achieve with the other locking schemes.

5.2 Closing the locking loop - piezo and current control

Regardless of which of the schemes is used, the underlying principle is a frequency-to-voltage converter. This voltage has then to be used to tune the wavelength of the laser. The goal is to achieve an error signal equal to zero, i.e. to have the desired frequency offset between the two lasers. Having a circuit that provides such an error signal, one has to think about possible ways of tuning the laser frequency according to the error signal.

A short introduction on possible ways of stabilising lasers is given in [40]. Thinking about the tools normally used to change the frequency of laser light, one might, for example, use an acousto-optical modulator (AOM) as a servo mechanism and counteract frequency fluctuations by changing the frequency applied to the AOM. The problem in this case is the slow response of the AOM, limited by the slow speed of sound between the acoustic transducer and the the part of the crystal through which the laser beam passes.

In our case we have grating stabilised laser diode systems for both the master and slave lasers. These allow easy change of the length of the extended cavity represented by the grating and the laserdiode itself via a piezo, as well as a fast current modulation via an implemented FET circuit. In the following, only ways of adjusting the wavelength by these means are considered.

5.2.1 Servo control of a piezo

In a grating-stabilised laser the first-order diffraction of a grating is reflected back to the laser diode, creating an extended cavity that allows only certain frequencies to be emitted. The extended cavity setup results in a linewidth of the emitted laser light of typically 1 MHz. The layout of this simple setup is shown in figure 5.7 on the next page.

By changing the distance between the grating and the laser diode, one changes the wavelengths allowed in the resonator. In order to be able to tune the distance in a relatively coarse way, a fine-thread screw can be used to roughly set the correct distance. The precision tuning is performed by a piezo crystal, which changes its length depending on the applied voltage and therefore tilts the grating. The ordinary procedure to optimise the emission of a certain wavelength is to set the screw in such a way, that light of roughly the right wavelength is emitted. Further optimisation is done by reducing the laser threshold at this distance via better back coupling of

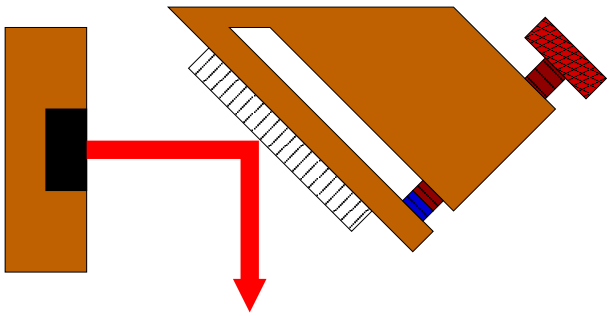

Figure 5.7: Schematic setup of a grating stabilised laser diode system (Littrow configuration). The first-order diffraction of the grating is coupled back to the laser diode, generating an additional cavity to precisely adjust the wavelength of the emitted light. The blue indicates the piezo crystal.

the first order diffracted light. This is done, together with the screw for horizontal backcoupling, by an additional screw that allows to tune the vertical position of the backreflected light. During all this optimisation, the piezo servo should be set to be in the middle of the available parameter space (normally about half of the maximum output voltage of the piezo servo control), to allow a large tuning range via the piezo after this first mechanical optimisation.

Once the laser is emitting light of roughly the right wavelength, one needs only to add the error signal (with appropriate sign and gain) to the voltage applied to the piezo. Then the slave laser should already start locking via the piezo of the grating.

A problem is that most of the time the error signal voltage is rather low compared to the voltages that are needed to properly drive the crystal. Therefore the error signal has to be amplified to an appropriate voltage region. Another problem that one might consider is: Feedback proportional to the error signal will cause a reduction of the error signal until it lies within a certain range of the set-point and is very small in magnitude. In order to adjust the wavelength even further with such a small error signal, one would like to integrate the small error signal and drive the piezo according to the integrated value. In addition, fast changes should be detected as quickly as possible, and be counteracted.

These problems can be solved by implementing a proportional–integral–differential (PID) servo control, which can easily be built from operational amplifiers, resistors and capacitors. It consists of a combination of three elements. The proportional part just amplifies the error signal to appropriate voltages. The integrator is capable of summing up the small error signal of an existing running lock and thereby enhances the precision of the lock. The third part is a differentiator, which can detect fast changes in the error signal and will compensate for them as well as possible.

The layout of the different elements of a PID regulator is shown in figure 5.8 on the facing page. With two simple rules for operational amplifiers, one can calculate the behaviour of the different parts [41]:

- The output attempts to do whatever is necessary to make the voltage difference between the inputs zero.
- The inputs draw no current.

Using these rules, one can calculate the output voltages for the inverting and non-inverting amplifier as well as the integrator and differentiator shown in figure 5.8 on the next page to be:

$$V_{\mathrm{out-non-inv}} = \left(1 + \frac{R_2}{R_1}\right) V_{\mathrm{in}} \tag{5.2}$$

$$V_{\mathrm{out-inv}} = -\frac{R_2}{R_1} V_{\mathrm{in}} \tag{5.3}$$

Regarding the inverting input of the integrator as a virtual ground, the output voltage of the integrator can be calculated to be:

$$V_{\mathrm{in}}/R = -C\frac{\partial V_{\mathrm{out-int}}}{\partial t} \tag{5.4}$$

which can be rewritten to

$$V_{\mathrm{out-int}} = \frac{1}{RC}\int V_{\mathrm{in}} dt + \mathrm{constant} \tag{5.5}$$

Using the same argument (inverting input at ground) for the differentiator, the input voltage produces a current $I = C\frac{\partial V_{\mathrm{in}}}{\partial t}$, resulting in an output voltage for the differentiator:

$$V_{\mathrm{out-diff}} = -RC\frac{\partial V_{\mathrm{in}}}{\partial t} \tag{5.6}$$

These operations on the input voltage can be combined in a circuit shown in figure 5.9 on page 48. The proportional gain performs the main regulation. At a critical gain, more gain will result in oscillations. Therefore the proportional gain should be below this threshold.

The small residual error signal after the optimised proportional feedback is summed by the integrator, resulting in additional servo signal. Again, too much gain in the integrator will result in oscillation, which has to be suppressed by setting the gain away from the threshold of oscillations.

The addition of a differentiator to the circuit, which tries to counter fast changes of the error signal, gives only a minor benefit. Most of the time the differential component is not used.

There are several ways of adjusting the gain and time constants of a PID. A possible way is to switch off the differential and integration parts, and increase the

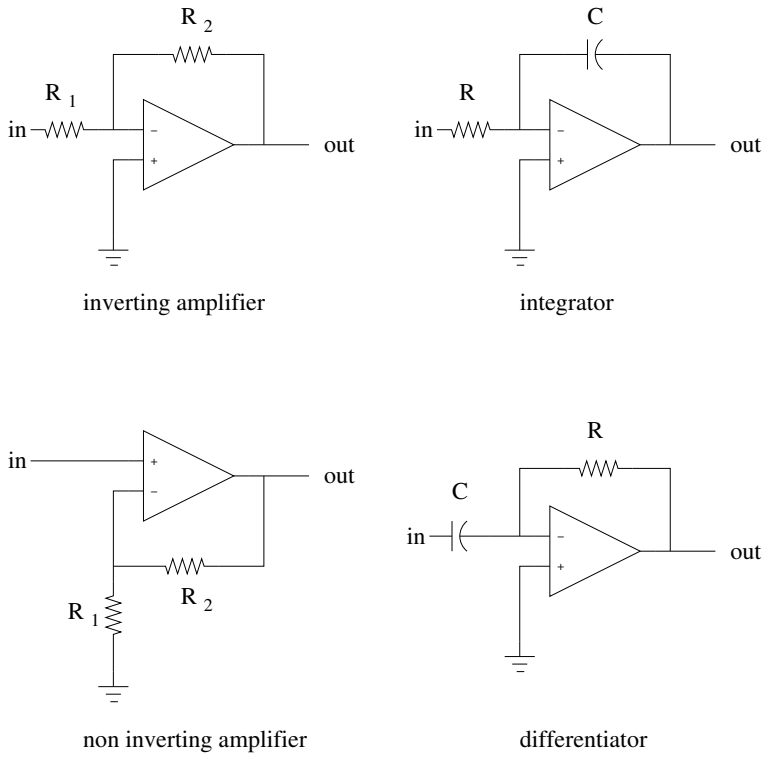

Figure 5.8: Proportional(inverting and non-inverting), integral and differential regulators

proportional gain until the error signal starts to oscillate. The frequency at which the signal oscillates is the critical frequency ν_{crit}. The proportional gain is then reduced until the oscillation ceases completely. The integrator time constant should then be set to correspond to a frequency that is 10 times smaller than ν_{crit}. The time constant of the differentiator should correspond to the same frequency as the critical frequency.

The bandwidth of the PID servo unit is limited by the chosen operational amplifiers and influenced by the time constants of the integrator and differentiator. Depending on the device used for adjusting the wavelength, there is rarely a need for high bandwidth op-amps, since the servo mechanism itself, such as a piezo, will be the limiting factor.

Using a piezo to adjust the wavelength via the grating will be by far the slowest control element in the whole setup as its bandwidth normally is in the region of some kHz. As piezo regulation is rather slow, one has to find other means to counteract fast fluctuations of the laser. Nevertheless, the piezo has one big advantage: It allows regulation long-term drifts, that can not be handled as easily by other electrical means.

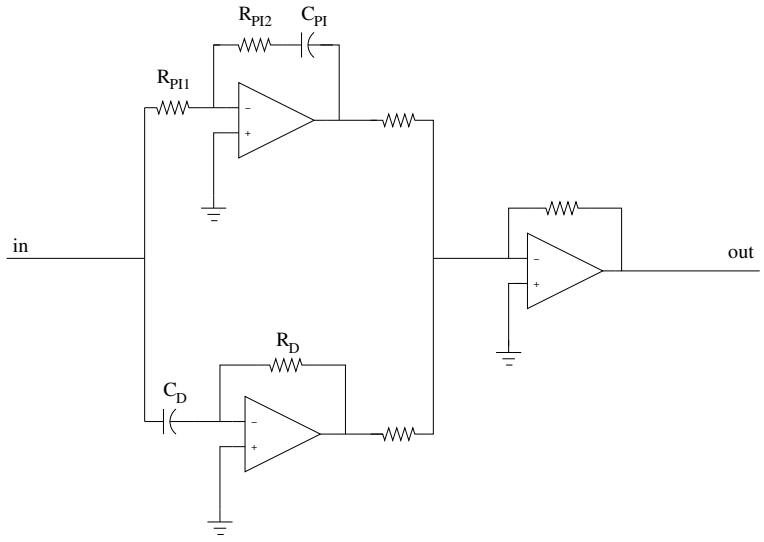

Figure 5.9: A possible layout of a combined PID regulator

5.2.2 Current control via a field-effect transistor

In addition to changing the voltage applied to the piezo, the wavelength of the emitted light can be changed in a much faster way by changing the current through the laser diode. A field-effect transistor (FET) in parallel to the laser diode and clamping the lasers current can perform the required current control, depending on the applied voltage.

A FET is a semiconductor device, which, as the name suggests, controls the current through a channel by an electric field produced by a voltage that is applied to the gate electrode. There is no additional current from the gate to the source, which would otherwise result in a biased current through the diode [41].

Using the circuit in the laser system from Toptica (see figure 5.10), an applied error voltage can have very fast influence on the current (for the DL100 system, the manual claims a bandwidth of the FET control of 5 MHz).

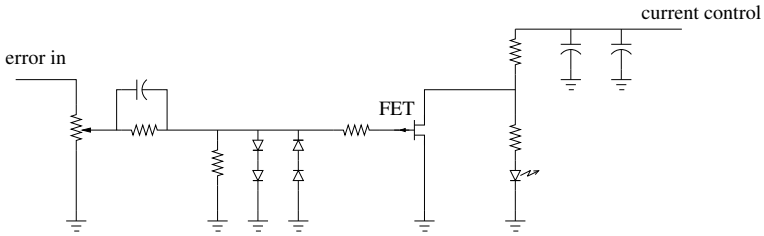

Figure 5.10: FET to control the diode current according to a Toptica DL100 system.

A big advantage of using a FET to change the current is the much greater bandwidth compared to the bandwidth of a piezo. One drawback of modifying the current are the small intensity fluctuations of the emitted light that may result in unwanted behaviour on other parameters of the experiment. One does not want

to have long term currents flowing through the FET. Together with the limited voltage range that can be applied to the FET, it is clear that current modulation offers only a limited possibility to counter long term drifts. Therefore, even if current modulation offers a very high modulation bandwidth, a piezo servo control should be implemented in addition.

A combination of PID servos for FET and piezo control seems to be optimal, but the settings for these elements have to be tested in the experiment, since the overall benefit strongly depends on the implemented devices and chosen parameters. Also, one needs to tailor the pertaining Bode plots to get the optimum results.

Chapter 6

Experimental setup of the offset lock

Considering the requirements (large capture range, high bandwidth, ability to produce a steep slope) for a good locking system system, the high-pass filter scheme presented in chapter 5 was chosen for our offset lock. This chapter will explain in more detail the functions of the circuit components, the influence they have on the behaviour of the error signal, and where the limitations of the circuit lie. Modification of different parts of the circuit were made, and the effect on the error signal was measured. Finally, the implementation of the lock is presented with detailed information about the components and measurements of the stability of the frequency offset.

6.1 Circuit layout

A detailed layout of the circuit is given in figure 6.1 on the next page. As all components are from MiniCircuits[1] , the labelling is taken according to the product name. The circuit can be divided into two parts, each consisting of two elements. One part gives a frequency dependent attenuation, followed by a power-to-voltage converter. The other part is an offset attenuation that is converted into a voltage. In both cases the power-to-voltage conversion is achieved by a combination of a diode followed by a low-pass. These voltages are finally added using resistors.

Looking at the circuit, it is obvious that the high-pass filter is the main component that has an output depending on the applied signal frequency at the input. One can regard the high-pass filter followed by the 'power-to-voltage' converter as a frequency-to-voltage converter. In this case, the slope of the high pass filter maps

[1]Mini-Circuits Europe Dale House: Wharf Road Frimley Green, Camberley, Surrey GU16 6LF, UK, http://www.minicircuits.com

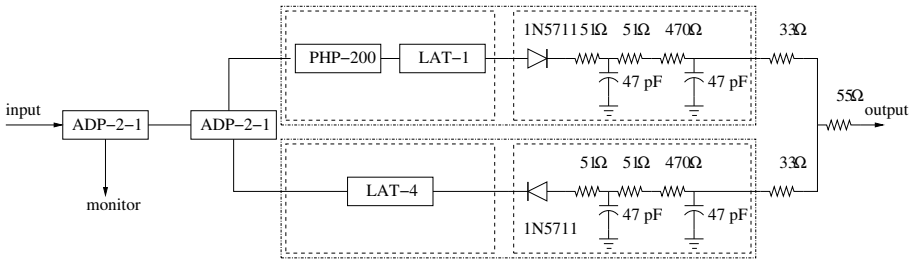

Figure 6.1: Schematic of the locking circuit: All components are from MiniCircuits. The ADP-2-1 is a SMD powersplitter. The PHP-200 is a surface mount high-pass filter with a defined 3 dB attenuation at 164 MHz. LAT-1 and LAT-4 are SMD attenuators with 1 dB and 4 dB attenuation.

directly to the slope of the error-signal. The high-pass filter requires, therefore, a steep linear slope in order to obtain linear behaviour around the lock frequency.

As discussed in the frequency-to-voltage converter scheme in section 5.1.1, one has to apply an offset voltage to obtain a zero voltage at a desired frequency. The offset voltage is generated by the attenuated input signal itself, that is converted into a voltage. The sign of the offset voltage is selected by the direction of the diode.

The reason for producing the offset voltage with a part of input signal is that it is crucial to the precision of the lock. The DC voltage after the high pass filter is strongly dependent on the power of the applied input signal. In order to have a lockfrequency independent of the input power, one must make the added offset voltage dependent on the power of the input signal. If not, the lock frequency would shift according to fluctuations of the input power. This technical problem is avoided by the use of the second path of the input signal. With the exception of the lack of a high-pass filter, the circuit is similar to that of the first path, producing a DC voltage with the same fluctuations but with opposite sign due to the inverted diode. In this way the fluctuations of the input power cancel each other. The zero point of the error signal should then not depend on the input power.

One minor problem remains: as the high pass filter operates as a frequency-to-power converter, fluctuations of the input power will be visible in the output voltage. While the setup suppresses lock frequency fluctuations, it cannot compensate for the influence of input power fluctuations on the output voltage. This effect is similar to fluctuations obtained by a proportional amplifier with amplification noise, affecting only the steepness of the error signal but not the zero point.

As a next step one has to look at the applied voltages. A reasonable input power of the beat signal is roughly 0 dBm, which corresponds to about 35 mV at the output of the circuit. Therefore, the error signal is amplified by two proportional amplifiers (one inverting, the other non-inverting) to obtain two error signals with voltages of opposite sign, with about ± 3 V for the non-inverted signal and about

∓ 1 V for the inverted error signal. This voltage region is useful as it ensures that one does not have to operate at the limit of gain of subsequent servo controls. The reason for implementing two output channel of the error-signal with different signs was to directly drive the piezo and FET control of the DL100 system. The two servo mechanisms cause opposite frequency shifts for a given input.

Looking at the schematic, most of the properties of the lock are determined by the high-pass filter. In our case, a MiniCircuits PHP200 was used. Its 3dB attenuation should occur at 164 MHz. This sets the lower end of the capture range to 2 times 164 MHz, equal to 328 MHz for negative frequency jumps. The reason for that is, that the mixer outputs only the frequency difference. This is equal to a mirrored error signal on the y-axis (compare with figure 6.2). For positive frequency jumps, the capture range is ideally infinity and only limited by the possibility of the diodes to rectify the signal. Further investigation on this topic will be done in the following.

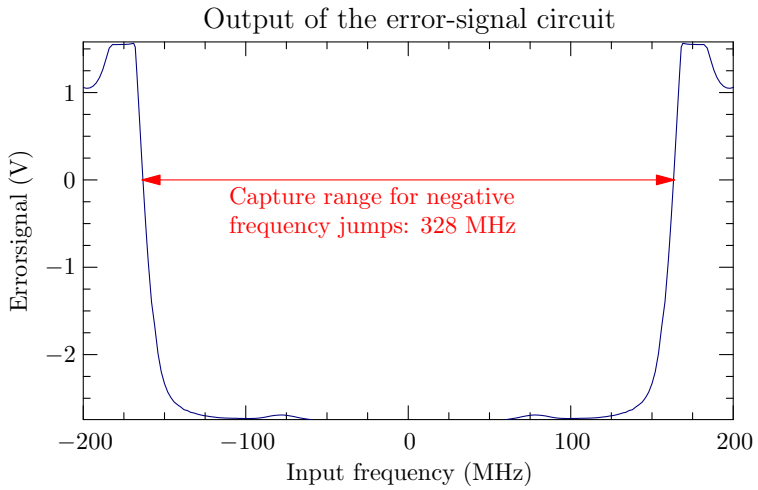

Figure 6.2: Explanation of the capture range of the circuit: The measured error signal has been mirrored on the y-axis, as the circuit is not dependent on the sign of the input frequency. Assuming that one locks to 164 MHz, only negative frequency jumps larger than 324 MHz will result in an error signal with a wrong sign for the servo control.

The capture range should be sufficient to handle any frequency jumps that might occur. The two attenuators have a difference of 3dB. The lock frequency is therefore expected to be 164MHz, depending on the exact 3dB attenuation of the PHP200 and the precision of the two attenuators.

A test device was built that allowed an initial investigation of circuit behaviour "on-the-fly", and enabled easy swapping of parts to quickly modify the output characteristics. The test device consisted of a soldered power-to-voltage converter as shown in Figure 6.1 on the preceding page and BNC pluggable devices (BHP-200, CAT-1 to CAT-8, ZSC-2-1). Figure 6.3 on the following page and 6.4 on page 55

show the behaviour of the error signal using different attenuators. The test circuit had a strong tendency for frequency pickup and resonances, so the evaluation circuit was rebuilt with SMD parts in a properly shielded case.

6.2 Frequency behaviour

Adjustments of the error signal can be made by changing the attenuators in the frequency dependent and offset voltage part. Measurements and results are shown in the following.

As previously explained, the path with the high-pass filter produces the error signal. The attenuator after the high-pass filter acts purely as a proportional amplifier. Increased attenuation should result in a reduction of the error signal, without producing any change in the voltage offset. Therefore, only the steepness of the slope should change. This effect was measured and verified. The error signal was investigated by applying frequencies from 50 MHz to 250 MHz (see Figure 6.3). The error signal drop for higher attenuation can clearly be seen. Small resonances at certain frequencies can also be seen, as a result of the not ideal test device. In the final circuit board, these resonances are suppressed, due to the appropriate soldering and additional shielding techniques.

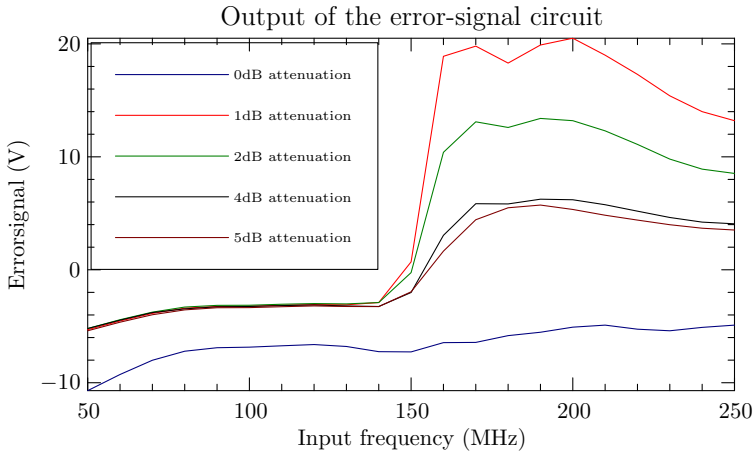

Figure 6.3: Behaviour of the error-signal for different attenuations after the high-pass. As expected, only the steepness of the slope changes, whereas the offset stays the same

If the attenuation in the other path (the path without the high pass filter) is increased, the power of the signal that is converted into the offset voltage is decreased. This should result in a shift of the whole error signal to higher voltages, without affecting the steepness of the error signal. This behaviour was tested and verified and the results are shown in figure 6.4 on the next page.

One would also expect to be able to change the lock frequency by changing the offset voltage via the attenuator. This is not really possible in the scheme, as the steepness of the slope at the lock frequency is to high. Even changes of several dB attenuation show only a small influence of a few MHz on the lock frequency. Nevertheless the influence is visible in the presented data (see figure 6.4).

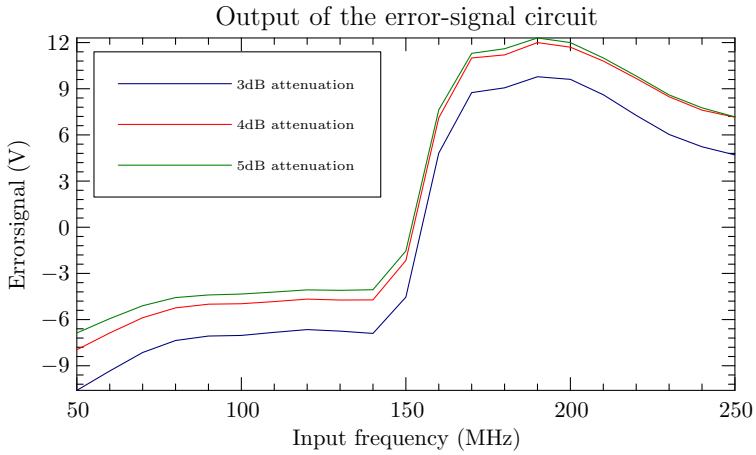

Figure 6.4: Behaviour of the error signal for different attenuations in the offset circuit. As described, only the offset of the error signal shifts, depending on the attenuation, while the steepness of the error-signal is not influenced.

The optimal attenuation values for both arms can be determined by considering the results obtained above and regarding the desired error-signal behaviour: As large an output voltage as possible, symmetric around the lock frequency. Therefore one should consider an additional attenuation of 1 dB in both arms, as it will only reduce the signal. It is similar in effect to adding a 1 dB attenuator directly in front of the power splitter. The important parameters are the difference between the attenuators and the value of the attenuator in the path without the high-pass filter.

In order to set the lock frequency to half way up the slope, the difference in attenuation between the two arms has to be 3 dB. Additionally, one would like to obtain as much signal as possible. Therefore low attenuation is used in the path without the high-pass filter.

The bandwidth of the circuit is ultimately set by the low-pass filter after the diodes. The larger bandwidth of the two servo mechanisms is that of the FET current control, with a bandwidth of 5 MHz. Therefore the low-pass filter is chosen to have a cutoff frequency of approximately that frequency. In our case a pair of low-pass filters is used to obtain a steeper slope, with a cutoff frequency at 6.44 MHz.

Figure 6.5 on the next page shows the error signal of the final circuit at an input power of -1 dBm. Despite a frequency behaviour of the error-signal equal to the attenuation characteristics of the high-pass filter, smaller resonances are visible

at 200 MHz, 350 MHz and 450 MHz. It is assumed that these are the result of component imperfections and capacitances in solder joints.

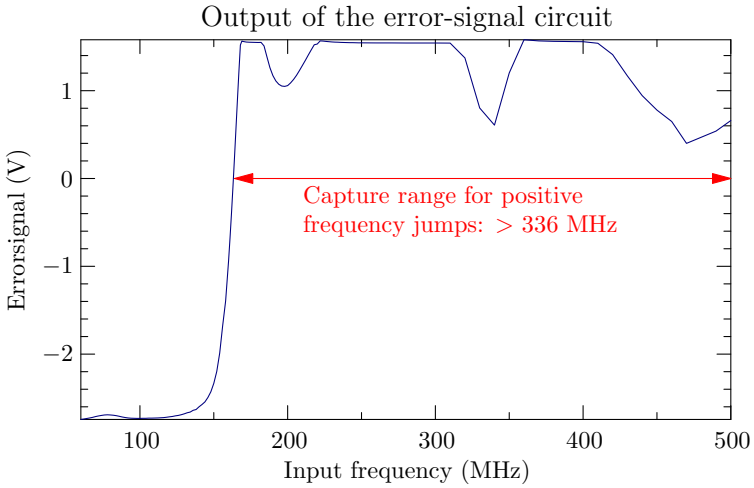

Figure 6.5: Error-signal produced by the circuit board at an input power of -1 dBm: The large capture range due to no other zero crossings of the error-signal is shown.

Investigating the frequency range of about 100 MHz above and below the lock frequency of the circuit (see figure 6.6 on the facing page), a linear slope is clearly visible. For the applied input power of -1 dBm, the slope is 0.2908 V/MHz. This value allows predictions of linewidth by the noise level of the error signal. The linear slope of the error signal stretches from about 159 MHz to 169 MHz, providing a linear dependence of the regulation for fluctuations of ± 4 MHz around the lock frequency.

6.3 Intensity dependence

The input signal is produced by the beat signal of two lasers on a photodiode. Should one or the other laser change its intensity, the input power of the circuit will change. The circuit is already designed to reduce the influence of intensity fluctuations on the lock frequency. However, it was important to investigate the effect of intensity fluctuations of the beat signal on the error signal and the lock frequency.

This was investigated by measuring the lock frequency as a function of input power. Figure 6.7 on the next page shows the results of the measurement. It can be seen that the optimal input power is in the region between -5 dBm and 2 dBm. The expected maximum intensity fluctuations are of the order of about ± 1 dBm under worst conditions, which would result in an uncertainty in lock frequency of below 25 kHz.

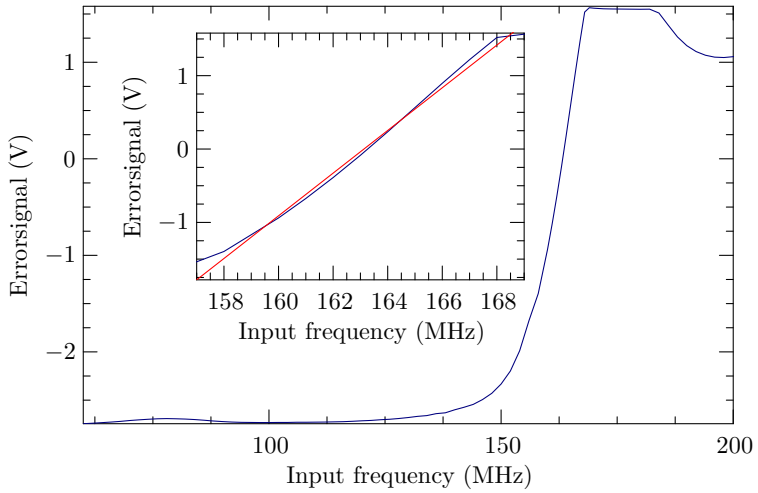

Figure 6.6: Error-signal produced by the circuit board: Around the lock frequency of about 164 MHz, a linear slope is measured, while the small resonance at about 200 MHz can be neglected as a possible influence on the locking behaviour. Such large frequency jumps are corrected by the proper sign of the error signal. The steepness of the slope is not affected. This measurement shows a slope of 0.29 V/MHz for an applied input power of -1 dBm.

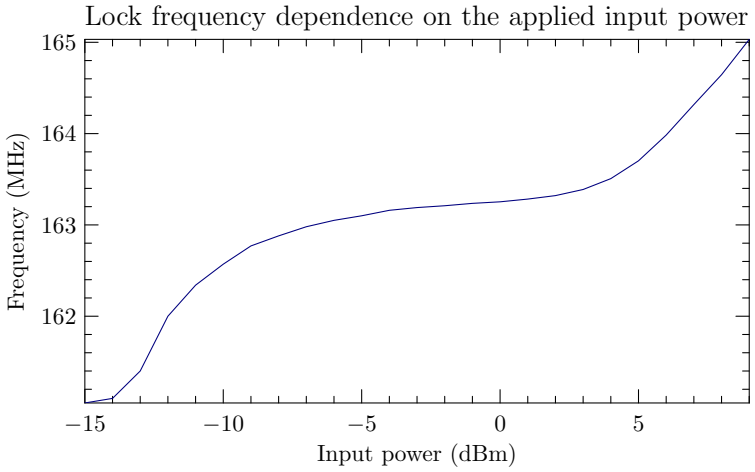

Figure 6.7: Influence of the input power on the lock frequency: For different input powers, the lock frequency of the device changes slightly. A small dependence can be found for input powers between -5 dBm and 2 dBm.

6.4 Technical details of the combined locking setup

The circuit discussed above forms the core of a well-defined offset lock of a slave laser from the reference laser. Nevertheless, the inclusion of several other devices in the lock loop, while inducing additional noise and drifts, can also lead to improvements. The following sections discuss the additional devices used.

6.4.1 The reference laser at 854 nm

The reference laser at 854.209 nm (the $P_{3/2} - D_{5/2}$ transition in $^{40}Ca^{+}$)is a Toptica DL100 grating-stabilised diode laser, stabilised to the TEM_{00} mode of a stable reference cavity using a Pound-Drever-Hall (PDH) locking scheme. Since this laser is the master laser and frequency reference, frequency fluctuations of this laser will be visible on the slave laser. The linewidth of this laser gives the lower bound for the linewidth of the slave laser.

It was not possible to measure the linewidth of the reference laser, as the necessary equipment was not available. Nevertheless, we can give information about the estimated linewidth of the lasers as we have observed in-lock beat signals of below 200 kHz between the offset laser and a home-made laser sytem, whose linewidth was previously measured to be $\approx$ 50 kHz [42] (see figure 6.8 on the facing page). This gives rise to the approximation that linewidths bigger than this resemble the convolution of two Gaussians with a linewidth equal to the linewidth of the reference laser. The linewidth is $1/\sqrt{2}$ of the observed linewidth of the beat signal.

6.4.2 PID and Scan control of the Toptica DL100 system

The slave laser system is a Toptica DL100, consisting of a rack including modules for temperature control, current control, scan control and a PID circuit connected to the scan control. Using the scan control, voltages from -5 V to +150 V can be applied to the piezo that drives the grating. The voltage is set by a 10-turn precision potentiometer on the front of the ScanControl. The feed forward from the scan control to the current control allows a frequency tuning without mode hops of up to 10 GHz at 850 nm (quoted from the Toptica manual). The linewidth of the free running laser is approximately 1 MHz.

The first step in setting up the laser for the first time is to apply 75 V to the piezo and adjust the grating via the fine-thread screw to emit laser light at a wavelength of approximately 854.209 nm. The Toptica system is mechanically very stable and usually the grating does not require further tuning.

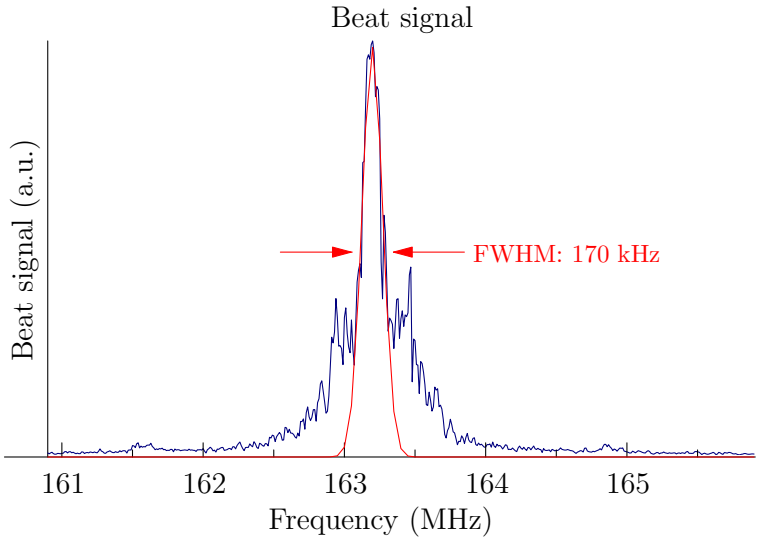

Figure 6.8: Lowest measured linewidth of a single shot beat signal (resolution bandwidth: 100 kHz, video bandwidth:10 kHz, sweep time: 10 ms): The linewidth of the reference laser was measured to be ≈ 50 kHz [42]. This measurement gives rise to the approximation that beat signal measurements with a larger linewidth result from a higher linewidth of the reference laser.

The locking loop is closed by connecting the error signal to the PID and activating the servo via the switch on the front. Optimisation of the PID circuit is usually performed by switching off different parts (i.e., proportional, integral and differential) in a defined sequence and optimising the gain at each stage, as presented in section 5.2 on page 44. Switches on the circuit board must be used to reduce the gain in different parts of the PID in order to find the proper settings, as only the integrator can be completely switched off. Another drawback of the design is that the setting of P, I, and D can only be adjusted via corresponding potentiometers from outside of the box. Therefore it is impossible to measure time constants of integration and differential part as well as the proportional gain. This means that one cannot record any of the settings of the PID parameters other than the overall gain.

As already mentioned, the additional influence of the scan control on the current via feed forward permits a large adjustment of the wavelength. However, the disadvantage is that during locking, in addition to adjustment of the piezo, the current also changes, resulting in intensity fluctuations. These can be seen on the beat signal. As a compromise the feed forward was reduced in order to suppress intensity fluctuations but still allow tunings of the laser without mode jumps of approximately 2 GHz.

6.4.3 Additional current control through a FET

The Toptica DL100 system allows the connection of the error signal directly to a FET, which can bias the current through the laser diode. This FET has a bandwidth of 5 MHz.

The FET could be controlled, in principle, by a PID system. However, the FET can and should be controlled very quickly as it is present to allow very fast feedback to the laser. The addition of an integral and/or differential part into the regulation would introduce an unwanted time constant. Any drifts of the frequencies (most likely due to grating drifts or minor temperature drifts) occur on a much longer timescale compared to the timescale on which the FET can act. Therefore these drifts should be compensated with a PID regulator via the Scan Control, and not by the FET. Large frequency changes corrected via the FET would require a large change of the diode current. This would result in a large change of the emitted laser intensity. In addition, the maximum voltage that should be applied to the FET is 1.4 V. For these reasons the FET control is only adjusted by a pure proportional amplifier.

Another reason not to include an integrator in both arms of the circuit is the possibility of a conflict between the PID and FET systems, which can occur if their reference voltages are not exactly alike. In this case, one would see a small offset, while the other would be at zero. This would result in additional fluctuations. As both circuits use different ways to set the setpoint and the reference voltage, this behaviour did occur during the examination of lock system properties. For short time scales the settings can be tuned to reduce the fight between the two integrators, however this problem is still observed if there are long term drifts on one of the reference voltages.

6.5 Linewidth of the locked laser

Figure 6.9 on the facing page shows the error signal of the free-running laser. Fluctuations of approximately 650 mV peak–to–peak can be observed.

Currently the sidebands for the Pound-Drever-Hall (PDH) lock of the master laser are applied directly by current modulation, and are therefore visible on the beat signal. Higher-order sidebands occur due to higher harmonics from the ZOS-50, used as an RF source for the PDH lock.

The beatsignal was observed on a spectrum analyser. A single shot spectrum of the PID-locked signal (i.e. no current modulation) is given in figure 6.10 on page 62.

A reduction of fluctuations by a factor of 8 can be obtained by applying the error signal to the FET control of the laser system (see figure 6.9). The residual fluctuations on the error signal are about 80 mV peak–to–peak.

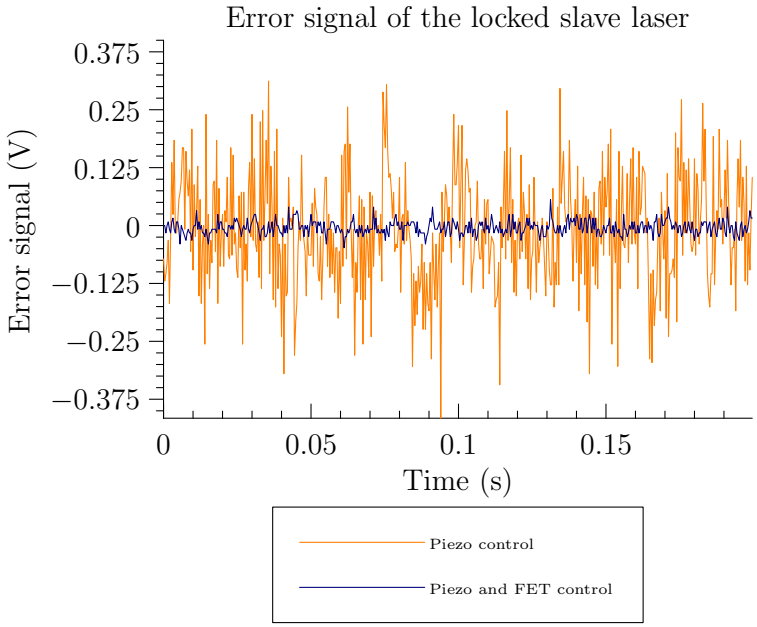

Figure 6.9: Improved lock due to the additional FET control. As the FET control is added, the error signal is reduced approximately by a factor of eight. The improved lock is also seen by the reduced width of the beat signal.

Taking the measured slope of the error signal at the lock frequency to be 5.52 MHz/V for an input power of about -5 dBm, a linewidth of roughly 450 kHz can be estimated. This value gives only a rough idea of the linewidth, as the measured powers differ by about 1 dB depending on which spectrum analyser is used (we used a Marconi Instruments, 100 kHz - 4.2 GHz, spectrum analyser 2383 with display 2380). The spectrum of the beat signal with piezo and current modulation is shown in figure 6.10 on the following page.

These single-shot spectra only give limited information about the stability of the offset lock, as long term fluctuations due to the short sweep time are not taken into account. To measure long term uncertainties on the timescale of minutes up to one hour, several spectra were taken, while the spectrum analyser was running in maximum–hold mode. The measured spectra are presented in figure 6.11 on page 63.

Knowing that the linewidth of the slave laser is limited by that of the master, we can estimate a lower bound for the slave lasers linewidth from the width of the beat signal. Assuming that the beat signal represents the convolution of two laser spectra of equal linewidth, the linewidth of either one will be $1/\sqrt{2}$ of the observed linewidth, equal to approximately 566 kHz for measurements on the timescale of one hour.

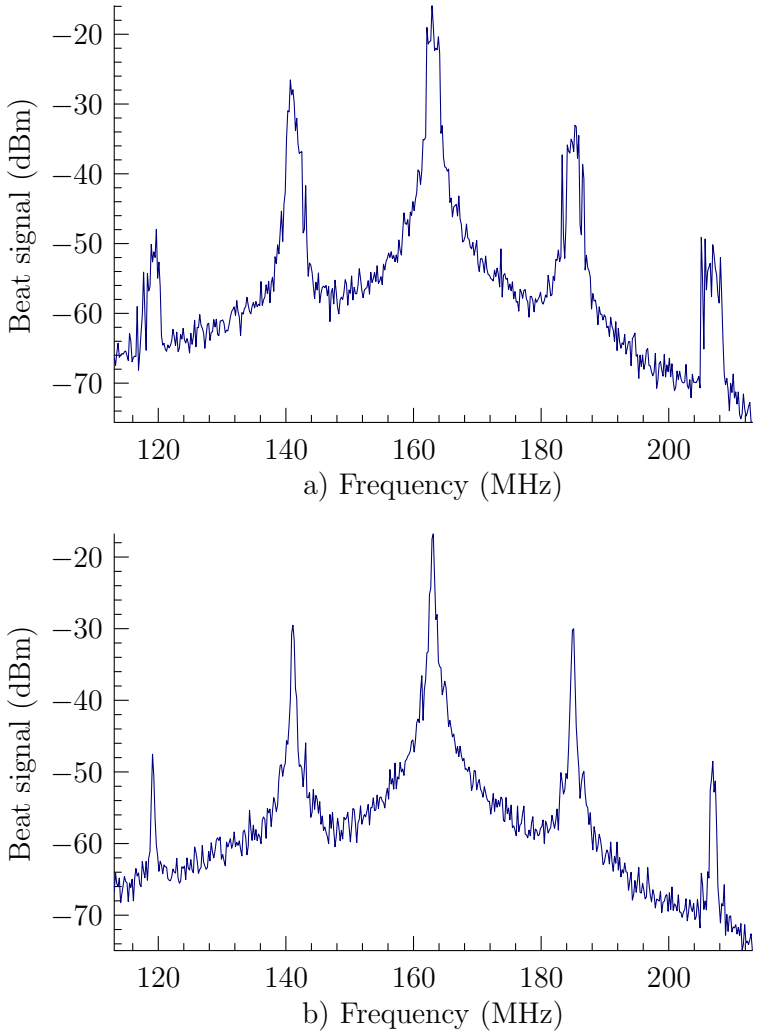

Figure 6.10: Single shot spectrum (resolution bandwidth: 10 kHz, video bandwidth: 10 kHz, sweep time: 1 s) of the beat signal without (a) and with (b) additional current modulation via the FET.

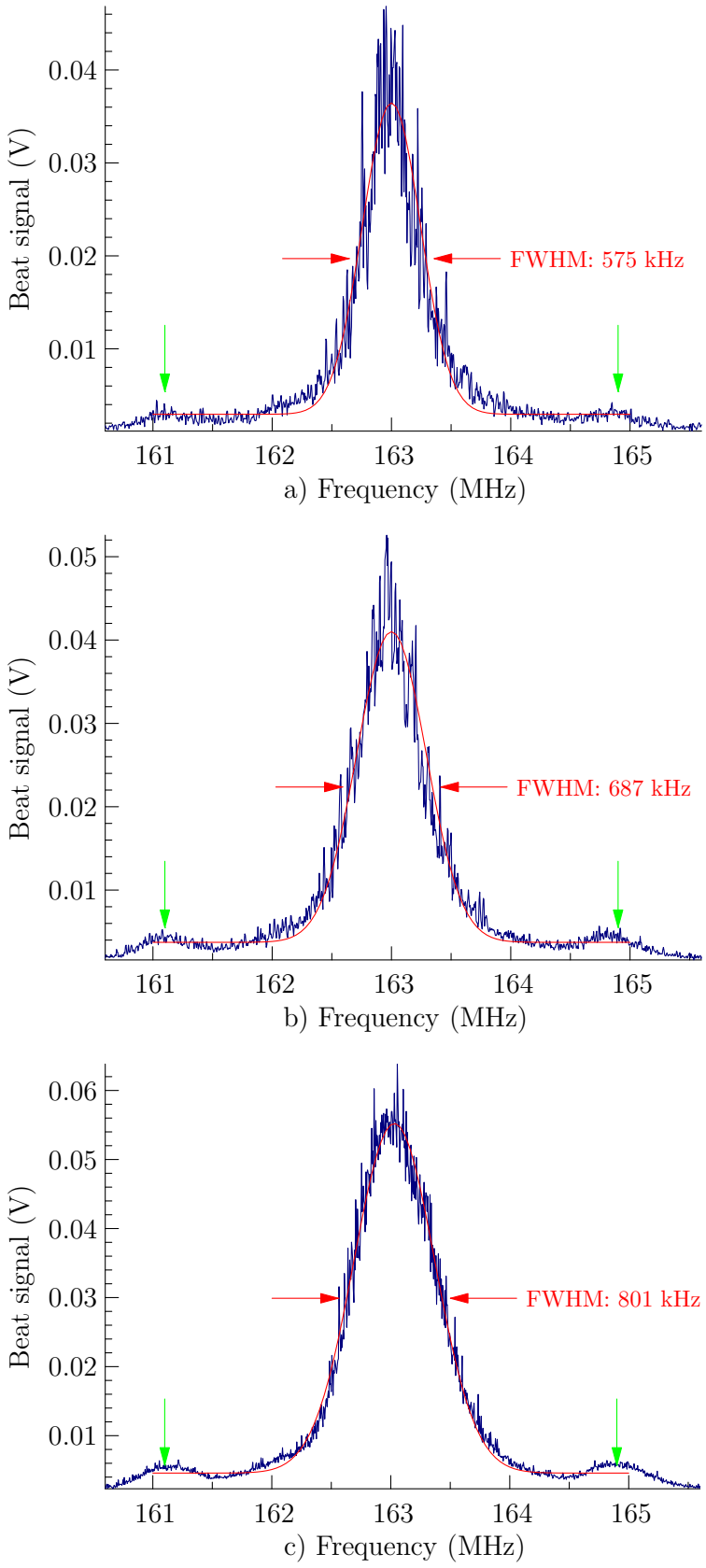

Figure 6.11: Maximum–hold spectrum (resolution bandwidth: 10 kHz) of the beat signal. The analyser parameters were: sweeptime 50 ms. For: a) 20 and b) 200 spectra taken. For c) the sweeptime was 5 s with 720 spectra recorded. The timescales are equal to 1 s, 10 s and 1 h. The green arrows indicate the pickup of a beat signal between the RF of one of the ion traps and the RF of the PDH lock.

6.6 Optical setup of the offset lock on the breadboard

The goal of the optical setup was to operate the offset lock on a small breadboard that includes fibre-coupled laser light from the two lasers. The emitted light of the frequency-offset laser is divided into three output channels: lock, wavemeter and experiment. In addition, an acousto-optical modulator was installed to allow fast switching of the output light going to the experiment.

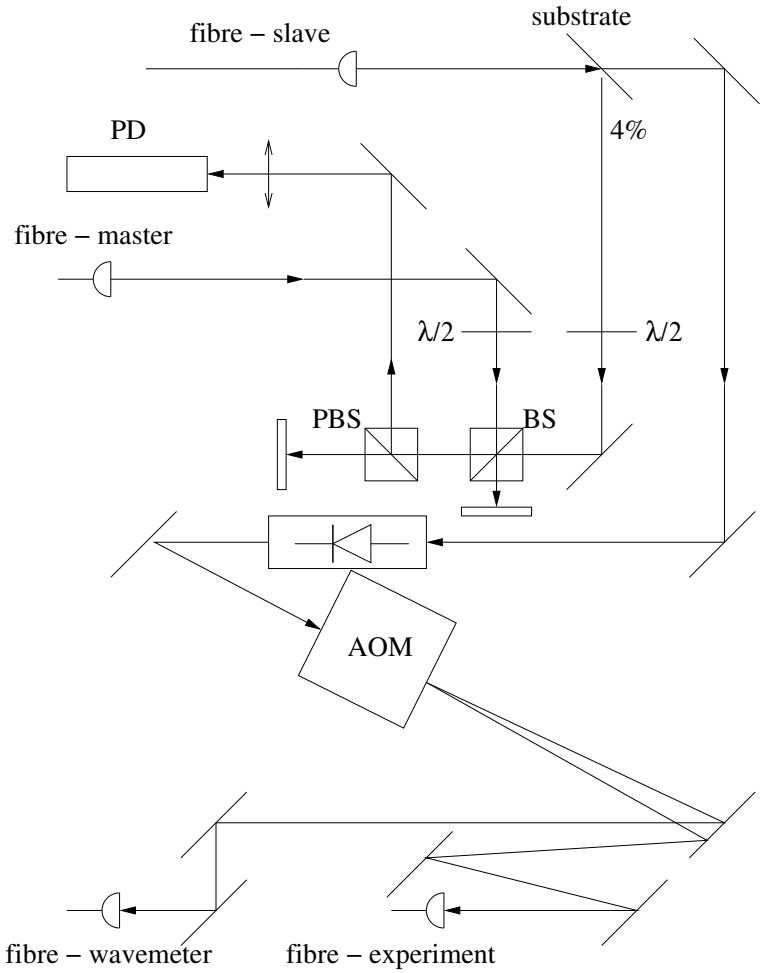

Figure 6.12: Layout of the breadboard of the offset lock. The labels represent: PBS - polarising beam splitter, BS - beam splitter, PD - photodiode. The optical diode is represented by the symbol known from electronics.

The beam path of the fibre-coupled Toptica DL100 system is shown in figure 6.12. A glass substrate is used to reflect about 4 % of the intensity, which is used to produce a beat signal with the master laser.

This pick-off is sent via two mirrors and a $\lambda/2$ waveplate to an ordinary beam splitter, where it is overlapped with the light from the master laser. A polarising

beam splitter is used to analyse the polarisation of the light and sent to the photodiode. The waveplates allow to optimise the polarisation of each beam in order to produce a large beat signal on the photodiode. Focused on the 1 GHz photodiode (electronics shop of the Institute for Experimental Physics) by a short focal length lens, a beat signal of about -5 dBm can be obtained.

The rest of the emitted light of the slave laser system is sent through an optical diode. The light is then coupled into an AOM in such a way that the first order of the light is shifted by -100 MHz. Therefore, the first-order diffracted beam can be quickly turned on and off by controlling the RF input of the AOM. Both beams, zeroth and first order, are sent to different fibre couplers. The zeroth order is sent to a wavemeter, while the first order is sent to the experiment.

The optical diode has to be used in order to reduce back-reflections of the first-order diffracted beam from the fibre. These would otherwise result in optical sidebands of twice the frequency of the RF signal that is applied to the AOM. Without the isolator a small portion of light is reflected from the face of the fibre that leads to the experiment. The frequency-shifted light passes through the AOM on its return path and is shifted in frequency further. Following the optical path back to the fibre output of the slave laser system, a small part is reflected and can produce sidebands to the beat signal. This behaviour has been observed as sidebands to the beatsignal at twice the frequency of the RF signal applied to the AOM. Blocking the first order diffraction of the AOM removed the sidebands. An optical isolator of 60 dB attenuation (Linos: FR 850 TS) was sufficient to allow the unblocking of the first-order diffraction.

6.7 Limiting factors

There are different limiting factors in the circuit. Besides the linewidth of the reference laser, there are electrical limitations in the setup that are not obvious at first glance. The following section will present some of the limitations and propose solutions to the problems.

6.7.1 A single-sideband mixer

The presented circuit produces an error signal for a given input frequency, with a zero output voltage at about 164 MHz. Nevertheless, the aim of the whole setup is to be able to tune the slave laser from about 100 MHz to about 1 GHz away from the atomic transition. Therefore the beat signal at the photodiode is mixed with a local oscillator that is set accordingly to produce the 164 MHz intermediate frequency for the closed loop.

The mixer will have output components at both the sum and difference frequencies of the inputs. This can easily be seen by multiplying two sine functions together and applying the appropriate trigonometric identities. In our experiment we are interested only in the difference. The properties of the mixer (ZAD-11) are such that the sum frequencies up to 600 MHz will be seen. Such sum frequencies will spoil the error signal. To eliminate this sum frequency, several possible solutions exist.

This problem strongly depends on the output frequency range of the mixer. For high frequencies, this problem most probably will not appear. For instance: for an offset of 500 MHz the sum of the frequencies will already be 1.164 GHz.

Another inherent feature of the setup that helps, is the use of an AOM. Using the first-order diffracted light of the acousto optical modulator, the effective lock frequency is increased. Assuming that the AOM reduces the frequency of the first order diffracted beam by ν_{AOM}, this has to be compensated by increasing the frequency of the local oscillator by the same frequency. As the local oscillator and beat signal frequency increase by ν_{AOM}, the sum frequency at the mixer increases by two times ν_{AOM}, while the difference frequency stays the same.

Depending on the mixer, this might still be a frequency that the mixer is able to transmit. A solution would be to add a low-pass filter after the mixer, with a 3 dB attenuation at about 400 MHz, therefore limiting the capture range for positive frequency jumps to about 150 MHz.

Another possibility would be to get rid of the higher frequency directly at the mixer. Such a mixer is called 'single sideband mixer'. It is able to provide either the sum or difference of the applied frequencies at the output [43].

The basic idea is to split the input signal, add a $\pi/2$ shift to one of the two paths, mix the signals with the local oscillator, shift one path again by $\pi/2$ and then add them at a power combiner. The layout of a single sideband mixer is shown in figure 6.13 on the next page.

The crucial device in the setup is the power splitter that produces the phase shift of $\pi/2$. In order to operate as desired, the phase shifter has to be able to shift both frequencies, difference and sum, by $\pi/2$ as precisely as possible. Comparing this condition for the phase shifters with the frequencies in our setup, they should be able to have a frequency range from about 100 MHz up to about 2.5 GHz. Usually, such devices are not available. Therefore, this interesting device can not be used.

As a single-sideband mixer can not be built according to the desired specifications, a low-pass filter after the mixer with a properly chosen cut-off frequency is the only available solution.

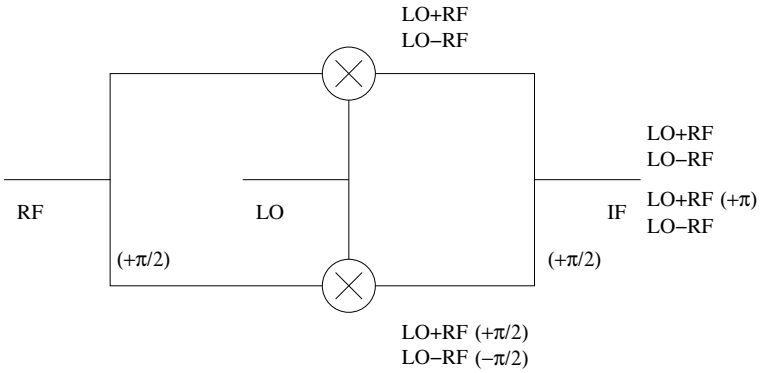

Figure 6.13: Basic layout of the circuit used as a single sideband mixer: The RF signal is split into two parts with a special powersplitter that also induces a phaseshift of $\pi/2$ on one part (the phase is indicated in brackets). These two signals are mixed with the local oscillator signal. Frequencies are subtracted and summed. Depending on the sign, also the phase shift is now either positive or negative. With a second power splitter and phaseshifter, the two IF signals of the mixers are summed. For the given setup, the sideband with the sum of the two frequencies is shifted by π and therefore will destructively interfere, while the sideband with the difference frequency will add.

6.7.2 Reducing intensity fluctuations

In section 6.3, the dependence of the lock frequency on the input intensity was shown (see figure 6.7 on page 57). The measured intensity fluctuations of about $\pm$ 0.5 dB result in an uncertainty of 25 kHz. This will directly increase the measured linewidth of the beat signal. Besides intensity fluctuations of the lasers, there is also another reason for intensity uncertainty at the circuit input. The amplifiers in the photodiode have different gains for different frequencies. The output power of the photodiode may vary by several dB between a lock at 100 MHz and 1 GHz. This is equivalent to a change of the proportional gain of the PID controller.

Intensity fluctuations at the input of the circuit may result from intensity fluctuations of one of the two laser beams due to current modulation, stress on a fibre, or electrical noise. Intensity fluctuations in the low frequency range can be counteracted by a laser intensity stabilisation with an AOM. High frequency fluctuations can not be regulated with the AOM due to its limited bandwidth. Therefore electronical power regulation schemes with a high bandwidth are presented. Either a limiter is used that is able to handle the necessary frequency range, or an amplifier is saturated so that input intensity fluctuations are not present at the output.

Using a PLS-2 power limiter, intensity fluctuations can be reduced by a factor of five, if the input power is between 3 and 8 dBm. This will also reduce the lock frequency uncertainty by a factor of five. In order to achieve the required input powers for the power limiter, an additional amplifier like a ZFL-500LN must be

inserted before the limiter.

Another way to reduce intensity fluctuations is to connect the mixed down signal with high power to a low noise amplifier. The input power must be chosen such that it does not harm the amplifier but forces the amplifier to saturate. As the amplifier is not able to provide more power, fluctuations should be reduced. The exact behaviour depends on the amplifier. A disadvantage of this approach is the truncation of the amplified signal, which leads to a change of the Fourier components of the signal

As the input signal ideally should not be altered in order to achieve a high input signal precision, the power limiter scheme was implemented. As a preamplifier, a ZFL-500LN was chosen. It can handle the output frequencies of the mixer as well as provide the required output power for the power limiter. A schematic of the complete electrical setup is shown in figure 6.14.

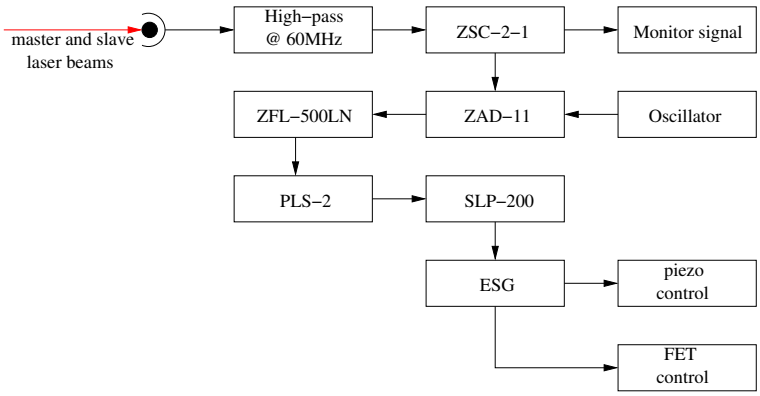

Figure 6.14: Electrical setup of the offset lock: The high-pass filter at the beginning must be used if the sidebands on the master laser for its Pound-Drever-Hall lock are also visible on the beam that is sent to the offset lock. The RF frequency, as well as higher harmonics of the RF source, can otherwise be observed in the spectrum. The beat signal is mixed down to an appropriate frequency with a ZAD-11 using a Marconi Instruments signal generator 2023 (9 kHz - 1.2 GHz) as an RF frequency source. The mixed down signal is amplified by a ZFL-500LN and power stabilised by a PLS-2. The SLP-200 with a cut-off frequency of 210 MHz is used to suppress the signal at the sum of the applied frequencies to the mixer. This filtered signal is connected to the error-signal generator (ESG) as shown in figure 6.1 on page 52 with its two output channels for piezo and FET control.

Chapter 7

Applications of the offset lock in the experiment

The experimental setup at the time of writing this thesis was not at a stage that allowed the investigation of Raman passages. Therefore, the frequency offset is presented and tested as frequency pointer – a tool to measure the most important properties of the cavity. This chapter shows results of measurements of the cavity length. These measurements are used to calculate other important properties of the cavity and thereby get an idea of the achievable parameters for the Raman transition.

7.1 Frequency pointer

A strong coupling between the atom and the cavity mode field is desired, represented by the parameter $\hbar g$, the interaction energy. Therefore a high field is needed, which can be achieved by reducing the mode volume of the cavity (see equation 4.29 on page 32 and figure 7.1 on the next page). This is done by separating the two mirrors of curvature R by a distance $L \simeq 2R$. No mode is supported for longer cavities while the mode volume rapidly increases for shorter cavities. Once the exact distance between the mirrors is known, the coupling strength and cooperativity can be easily calculated.

One possible way to estimate the distance between the mirrors is to use a laser-beam with sidebands, that are, for example, applied to the beam via an electro-optical modulator (EOM). Sending this beam through the cavity and scanning the cavity length, the transmission signal shows several modes of the cavity. The sidebands on the carrier can be used to scale the frequency range. This allows the calculation of the free spectral range, and thus the length of the cavity.

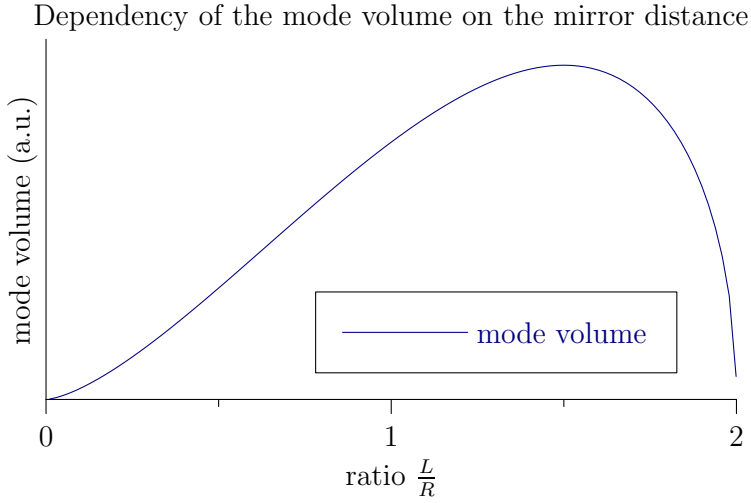

Figure 7.1: Mode volume of the cavity depending on the mirror distance

The technical problem in doing this is the scanning technique. Normally, the cavity length is tuned by a piezo, which is connected to an AC signal. A piezo crystal, however, has a nonlinear length dependence on the applied voltage. Therefore the free spectral range obtained by estimating the mode spacing via the sidebands on the carrier can only be used as a rough approximation.

A better way to measure the distance is to send light of tunable frequency through the cavity, and simply scan the frequency of the light to measure frequencies at which light passes through the cavity. The frequency distance between the modes allows the precise calculation of the cavity length. This represents a possible application for the frequency offset lock.

7.1.1 Mode spectrum of a cavity

Higher order Gaussian beam modes with m and n zero-field crossings (nodes) in a plane perpendicular to the cavity axis can be supported by the cavity. These modes are referred to as transversal-electrical modes (TEM), where indices represent the number of zerocrossings of the transverse field. More information on this topic can be found in [26].

The phases of the mode have to match in a way that interference doesn't destroy the mode as the light is reflected several times in the cavity. Considering spherical mirrors, this can be described by fulfilling:

$$\theta_{m,n}(z_1) - \theta_{m,n}(z_2) = q\pi \tag{7.1}$$

$\theta(z)$ represents the phase shift depending on the location along the axis, z_1 and z_2 describe the position of the mirrors. q is an integer. Phase shifts at the mirrors, equal to π, are neglected as they can be included in the term $q\pi$.

For a given transversal-electrical mode (TEM), the phase shift is given by [44]:

$$\theta(z) = kz - (m + n + 1)\tan^{-1}(z/z_0) \tag{7.2}$$

with

$$z_0 = \frac{\pi\omega_0^2 n_0}{\lambda} \tag{7.3}$$

ω_0 is the waist of the beam, while n_0 represents the index of refraction.

Inserting equation 7.2 into the resonance condition and using $L = z_2 - z_1$, the following formula is obtained:

$$k_q l - (m + n + 1)\left(\tan^{-1}\left(\frac{z_2}{z_0}\right) - \tan^{-1}\left(\frac{z_1}{z_0}\right)\right) = q\pi \tag{7.4}$$

From this equation follows that:

$$k_{q+1} - k_q = \frac{\pi}{l} \tag{7.5}$$

Using $k = \frac{2\pi\nu n_0}{c}$, the free spectral range of a cavity can be calculated to be

$$\nu_{q+1} - \nu_q = \frac{c}{2n_0 l} \tag{7.6}$$

while the frequency spacing for various transverse mode indices is given by:

$$\Delta\nu = \frac{c}{2\pi n_0 l}\Delta(m + n)\left(\tan^{-1}\left(\frac{z_2}{z_0}\right) - \tan^{-1}\left(\frac{z_1}{z_0}\right)\right) \tag{7.7}$$

The interesting part in this equation represents $\Delta(m+n)$, that depends only on the change of the sum of the indices of the transverse modes.

Equation 7.7 can be simplified by introducing reasonable restrictions. Using mirrors with the same curvature, the centre will be in the middle of the cavity. Therefore the position of the mirrors will be $\pm L/2$. Taking the previously introduced definition of $\Delta L = 2R - L$, the frequency dependency of the resonant frequencies for different transverse modes is:

$$\Delta\nu = \frac{c}{\pi n_0 L}\Delta(m + n)\arctan\left(\sqrt{\frac{L}{\Delta L}}\right) \tag{7.8}$$

These equations have been derived for a near planar mirror setup. Regarding the evolution of the mode spacing for a change from near planar to a near confocal resonator in figure 7.2 on the following page, a change in the mode numbering is required. To obtain the normally measured mode spacing for a near concentric resonator, an integer j, equal to the mode value indicated in the figure, times the free spectral range has to be subtracted from the mode spacing given in equation 7.8, resulting in a transverse mode spacing of

$$\Delta\nu_{\text{nearconcentric}} = \frac{c}{2\pi n_0 L}\Delta(m + n)\left(\pi - 2\arctan\left(\sqrt{\frac{L}{\Delta L}}\right)\right) \tag{7.9}$$

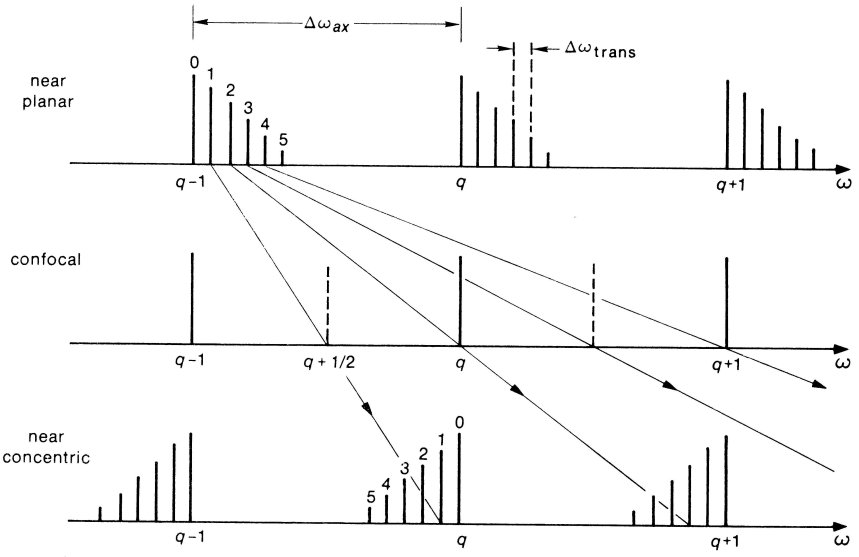

Figure 7.2: Transverse and longitudinal modes of a cavity, for different geometries. $\Delta\omega_{\mathrm{ax}}$ represents the free spectral range of the cavity. $\Delta\omega_{\mathrm{trans}}$ is the frequency difference between different TEM modes of the cavity. As the distance between the mirrors is increased, $\Delta\omega_{\mathrm{trans}}$ becomes bigger, until higher TEM modes "jump" to another free spectral range. Taken from [26].

To provide an idea of the scale of different cavity parameters and how they depend on the distance of the mirrors, several parameters have been calculated for different mirror distances in table 7.1 on the facing page. A significant change in the parameters can only be seen when the distance between the mirrors is close to the critical length of twice the curvature.

7.1.2 Measurement results of the cavity length

The cavity length was stabilised via a Pound-Drever-Hall lock setup to the light of a cavity-stabilised 785 nm laser. The light of the 854 nm frequency offset laser system was superposed with the light at 785 nm. To separate these two wavelengths, a dichroic mirror was placed at the exit of the cavity. The light of the 854 nm laser was then split into two parts: one part is sent to a CCD chip to show the Gaussian mode profile, the other one to a photodiode to see the transmission signal.

The cavity length, the offset lock and the wavelength of the master laser were adjusted in such a way that the frequency of the light at 854 nm was already near to that of a TEM_{00} mode of the cavity.

Locking the cavity to the 785 nm laser, the frequency of the local oscillator of the offset lock was tuned until the TEM_{00}-mode of the cavity was found. Increasing the frequency of the local oscillator, the TEM_{01}- and the TEM_{10}-modes were also

mirror distance (mm)	19.90	19.95	19.99
mode spacing (MHz)	339.364	239.27	106.75
beam spot size (centre) (μm)	13.85	11.65	7.80
beam spot size (mirror) (μm)	195.85	233.05	348.67
mode volume (10^{-3} mm^3)	3.00	2.13	0.95
coupling strength g (2π MHz)	1.51	1.79	2.68
cavity decay κ ($2\pi 10^{-2}$ MHz)	4.829	4.816	4.807
cooperativity	1.088	1.536	3.432
fraction of coupled photons	0.685	0.754	0.873

Table 7.1: Several parameters of the cavity depending on the distance between the mirrors. A curvature of 1 cm is chosen. The wavelength is set to be 854.209 nm with a cavity finesse of 78000.

observed. Using the formula presented above, the cavity length and its important properties for the experiment were then calculated. A table presenting these values is shown in table 7.3 on the next page.

	Frequency (MHz)
00-mode	825.3(1)
01-mode (left-right)	1136.3(1)
10-mode (top-bottom)	1129.4(1)

Table 7.2: Frequencies of the local oscillator at which Gaussian modes of the cavity were visible

A conflict encountered in these results is the disagreement of the cavity length within the calculated error. It is assumed that the disagreement results from a slightly imperfect mirror setup. Therefore the normally degenerated TEM_{01}- and TEM_{10}-mode split.

The measurement of the cavity length shows that a coupling rate of about 1.5 MHz can be expected. Together with the cavity photon leakage of about (2π) 50 kHz and a $\gamma_{\mathrm{non-trans}}$ that is equal to (21.51 + 1.576) MHz, the condition for the 'bad cavity regime' $\gamma_{\mathrm{non-trans}} \ll g^2/\kappa \ll \kappa$ within the weak coupling regime can not be fulfilled. The reason is that the finesse of the cavity is too high, resulting in a small κ. In addition, the strong decay of the $P_{3/2}$ to the $S_{1/2}$ state induces additional high leakage of photons that do not couple to the cavity mode, represented by a large $\gamma_{\mathrm{non-trans}}$.

Nevertheless, a cooperativity bigger than 1 is obtained. This means that interaction processes between the cavity and the atom are faster then other dissipative processes. It indicates the possibility for coherent interaction, probably allowing the experimental setup to be used for future experiments converting stationary to flying

	00-01 mode	00-10 mode
mode spacing (MHz)	311.0(1)	304.1(1)
cavity length (mm)	19.9159(5)	19.9195(5)
beam waist (centre) (μm)	13.27(2)	13.12(2)
beam waist (mirror) (μm)	204.5(3)	206.8(3)
mode volume (10^{-3} mm^3)	2.753(8)	2.693(9)
coupling strength g (2π MHz)	1.781(2)	1.800(3)
cavity decay κ ($2\pi 10^{-2}$ MHz)	4.825(1)	4.824(1)
cooperativity	1.516(5)	1.549(5)
fraction of coupled photons	0.752	0.756

Table 7.3: Final properties of the cavity calculated by the frequency difference between different modes. The TEM_{01}-mode represent horizontally aligned intensities, the TEM_{10}-mode represents vertical aligned intensity. A difference between the two measurements of the cavity length of 4 μm was found.

qubits. For such experiments one would perform a π pulse with a Raman passage from state $\mathrm{S}_{1/2}$ to $\mathrm{D}_{5/2}$ and wait until the photon is emitted out of the cavity. One would like to have a rough idea what the effective Rabi frequency between those two states is. Assuming a laser beam with a power P of 1 mW, focused at the position of the atom with a waist w of 30 μm, one can calculate the Rabi frequency $\Omega_{\mathrm{S-P}}$ for the S-P transition. The Wigner coefficient for this transition is $\sqrt{3/8}$. Calculating the electric field with

$$\rho_{\mathrm{energy}} = \frac{2P}{w^2\pi} \tag{7.10}$$

$$E = \sqrt{\frac{2\rho_{\mathrm{energy}}}{\varepsilon_0 c}} \tag{7.11}$$

the Rabi frequency for the resonant S-P transition is calculated to be

$$\Omega_{\mathrm{S-P}} = 435.9\ (2\pi)\ \mathrm{MHz} \tag{7.12}$$

Assuming a detuning of 100 MHz, an effective Rabi frequency of 3.9 MHz with $\gamma_{\mathrm{non-trans}} = 3.4$ MHz is obtained. Due to the small κ, this leads to the effective strong coupling regime.

In order to achieve the desired bad cavity regime, one needs an effective coupling that is smaller then κ. g is fixed by the cavity, therefore $\Omega_{\mathrm{S-P}}$ has to be reduced via the intensity of the 393 laser. An intensity of 10 μW leads to a Rabi frequency of 43.6 MHz. A frequency offset of 810 MHz results in fulfilment of bad cavity conditions, although at the cost of an effective Rabi frequency of 48.17 kHz.

The conclusion of these final calculations is, that the experiment will be operated between strong coupling and bad cavity regime. Depending on the available power

of the 393 laser, one has to find a compromise between large effective Rabi frequency and bad cavity regime with single photons leaking out of the cavity.

Chapter 8

Conclusions and outlook

The aim of this work was to set up a laser system to perform a high precision frequency offset with respect to a reference laser.

Basic theory of state transfer in two and three level systems via light interaction was introduced. Further detail of the possibilities to coherently move population between the two ground states in Λ systems was then presented. The use of a Raman transition with a frequency offset was introduced as a possible means of single photon production. Coherent interaction of light and states is possible due to suppressed spontaneous decay because of the frequency offset.

This was followed by an explanation how $^{40}Ca^{+}$ can be idealised as a three level scheme in a suitable experimental setup. Techniques for ion trapping and cooling were introduced, together with an explanation how the ion couples to the cavity field.

In order to lock the cavity to a frequency equal to a defined offset to an atomic transition of $^{40}Ca^{+}$, a frequency pointer must be built. As a reference, a laser emitting light at a wavelength equal to the atomic transition is used. Different approaches to performing an offset lock from this wavelength were discussed. We conclude that electrical error-signal generation via the beat signal of master and slave laser on a photodiode is most suitable. Compared with other schemes for error-signal generation, a high-pass filter scheme shows superior properties.

The circuit has been implemented and connected to the laser setup and its properties have been measured. The circuit can handle negative frequency jumps of 324 MHz and, ideally, infinite positive frequency jumps limited only by the diodes' ability to rectify the signal. Beat signal linewidths of below 200 kHz have been observed, apparently limited by the larger linewidth of the reference laser. Maximum-hold spectra show offset-frequency uncertainties of about 566 kHz on the time scale of one hour, again limited only by the precision of the reference laser. For the given setup, we are able to perform frequency offsets from approximately 0 MHz up to about 1 GHz. These specifications are limited only by the frequency range of the

installed photodiode.

This setup has been used to measure the frequency spacing between different modes of the near-concentric cavity. The length of the cavity has been measured with a precision of 10^{-7} m. This value for the cavity length allowed the calculation of all the experimentally important cavity parameters. The important conclusion of these calculations was the estimation that the experimental setup should be able to fulfil the effective strong coupling requirement for a frequency offset of 100 MHz and with an effective Rabi frequency between the $S_{1/2}$ and $D_{5/2}$ levels of 3.76 (2π) MHz. With a relatively low Rabi frequency of 48.17 kHz, the experiment can also be operated in the bad cavity regime.

Currently, the capture range of the frequency offset lock is limited due to two reasons. The Pound-Drever-Hall (PDH) lock of the reference laser uses sidebands directly on the emitted light. These sidebands are visible on the beat signal and detected by the offset lock circuit. The second reason is the mixer itself. The intermediate frequency of the output signal can be both a difference and a sum frequency, and the sum frequency will spoil the error signal. Both problems are solved at the moment by a bandpass filter, consisting of a low-pass to reduce the sideband signal of the master laser and a high-pass filter to suppress the higher intermediate frequency signal of the mixer. These filters unfortunately limit the capture range of the offset lock.

In order to get rid of the low-pass filter, the sidebands for the PDH lock will only be applied to the light needed for the error signal generation of the PDH via an electro-optical modulator. This will result in a sideband-free carrier reference signal, that will be sent to the frequency offset lock.

In order to remove the high-pass filter, one has to make sure that the mixer does not output the higher sideband intermediate frequency. It has been explained, that a feature of the installed acousto-optical modulator (AOM) is the need to change the applied frequencies to the mixer according to the frequency shift by the AOM. Replacing the current AOM with a model that operates at 200 MHz, we could remove the the high-pass filter.

These changes would result in the above-mentioned capture range of 364 MHz for negative and ideally infinity for positive frequency jumps.

Finally one would like to find the minimum lock frequency uncertainty of the circuit, which can be done by using a reference frequency with a narrow linewidth of below 50 kHz. This may be done in the future using an ultra stable reference cavity for the PDH lock of the reference laser.

Bibliography

[1] E.T. Jaynes and F.W. Cummings. *Proc. IEEE*, 51:89, 1963.

[2] P. Stehle. Atomic radiation in a cavity. *Physical Review A*, 2:102, 1970.

[3] G. Barton. *Proceedings Royal Society London A*, 320:251, 1970.

[4] D. P. DiVincenzo. The physical implementation of quantum computation. *Fortschritt der Physik*, 48:771–783, 2000.

[5] F. Schmidt-Kaler, H. Haeffner, M. Riebe, S. Gulde, G.P.T. Lancaster, T. Deuschle, C. Becher, C.F. Roos, J. Eschner, and R. Blatt. Realization of the Cirac-Zoller controlled-NOT gate. *Nature*, 422:408–411, 2003.

[6] S. Gulde, M. Riebe, G.P.T. Lancaster, C. Becher, J. Eschner, H. Haeffner, F. Schmidt-Kaler, I.L. Chuang, and R. Blatt. Implementing the Deutsch-Josza algorithm on an ion-trap quantum computer. *Nature*, 421:48–50, 2003.

[7] J.I. Cirac, P. Zoller, H.J. Kimble, and H. Mabuchi. Quantum state transfer and entanglement distribution among distant nodes in a quantum network. *Physical Review Letters*, 78:3221–3224, 1997.

[8] P. Zoller. Lecture on quantum optics. 2003/04.

[9] R. Loudon. *The Quantum Theory of Light*. Oxford Science Publications, second edition, 1983.

[10] B.W. Shore. *The Theory of Coherent Atomic Excitation*, volume two. Wiley-Interscience Publication, New York, 1990.

[11] K. Bergmann, H. Theuer, and B.W. Shore. Coherent population transfer among quantum states of atoms and molecules. *Review of Modern Physics*, 70:1003–1025, 1998.

[12] J.R. Kuklinski, U. Gaubatz, F.T. Hioe, and K. Bergmann. Population transfer in a three-level system driven by delayed laser pulses. *Physical Review A*, 40:6741–6744, 1989.

[13] M.P. Fewell, B.W Shore, and K. Bergmann. Coherent population transfer among three states: Full algebraic solutions and the relevance of non adiabatic processes to transfer by delayed pulses. *Australian Journal of Physics*, 50:281–308, 1997.

[14] C.D. Fidio, S. Maniscalco, W. Vogel, and A. Messina. Cavity QED with a trapped ion in a leaky cavity. *Physical Review A*, 65:33825, 2002.

[15] C. Maurer. Kontrolle der Einphotonenemission eines einzelnen Ca-Ions. Master's thesis, Universität Innsbruck, 2004.

[16] I. Marzoli, J.I. Cirac, R. Blatt, and P. Zoller. Laser cooling of trapped three-level ions: Designing two-level systems for sideband cooling. *Physical Review A*, 49:2771–2779, 1994.

[17] P. Meystre and M. Sargent. *Elements of Quantum Optics*. Springer Verlag, New York, 1998.

[18] D.F.V. James. Quantum dynamics of cold trapped ions with application to quantum computation. *Applied Phyics B*, 66:181–190, 1998.

[19] T. Mayer-Kuckuk. *Atomphysik*. B.G. Teubner Stuttgart, fourth edition, 1994.

[20] W. Paul. Quadrupole mass filter. *Zeitschrift für Naturforschung A*, 8:448, 1953.

[21] P.K. Ghosh. *Ion Traps*. Clarendon Press, 1995.

[22] D.J. Berkeland, J.D. Miller, J.C. Bergquist, W.M. Itano, and D.J. Wineland. Minimization of ion micromotion in a Paul trap. *Journal of Applied Physics*, 83:5025–5033, 1998.

[23] T. Haensch and A. Schawlow. Cooling of gases by laser radiation. *Opt. Comm.*, 13:68, 1975.

[24] D.J. Wineland and H.G. Dehmelt. Proposed $10^{14}\Delta\nu < \nu$ laser fluorescence spectroscopy on Tl^+ mono-ion oscillator iii (side band cooling). *Bull. Amer. Phys. Soc.*, 20:637, 1975.

[25] R. Blatt. Laser cooling of trapped ions. *In: Fundamental Systems in Quantum Optics, Ed. J.Dalibard, J.M.Raimond and J.Zinn-Justin, Elsevier Science Publishers B.V., Les Houches, Session LIII*, pages 253–286, 1990.

[26] A.E. Siegman. *Lasers*. University Science Books, Sausalito, 1986.

[27] P. Grangier, G. Reymond, and N. Schlosser. Implementation of quantum computing using cavity quantum electrodynamics schemes. *Fortschritte der Physik*, 48:859–874, 2000.

[28] R.D. Cowan. *The theory of atomic structure and spectra*. University of California press, 1981.

[29] P.R. Berman, editor. *Cavity Quantum Electrodynamics*. Academic Press, San Diego, 1994.

[30] Q.A. Turchette, R.J. Thompson, and H.J. Kimble. One-dimensional atoms. *Applied Physics B*, 60:1–10, 1995.

[31] E.M. Purcell, H.C. Torrey, and R.V. Pound. Resonance absorption by nuclear magnetic moments in a solid. *Physical Review*, 69:37–38, 1946.

[32] R.W.P. Drever, J.L. Hall, F.V. Kowalski, J. Hough, G.M. Ford, A.J. Munley, and H. Ward. Laser phase and frequency stabilization using an optical resonator. *Applied Physics B*, 31:97–105, 1983.

[33] A.B. Mundt. *Resonator QED with Single Trapped Ca^+-Ions*. PhD thesis, Universität Innsbruck, 2003.

[34] K. Szymaniec, S. Ghezali, L. Cognet, and A. Clairon. Injection locking of diode lasers to frequency modulated source. *Optics Communications*, 144:50–54, 1997.

[35] R.B.M Clarke, E. Riis, G.P. Barwood, P. Gill, G. Huang, and H.A. Klein. A sideband-injection locked extended cavity diode laser for interrogating cold trapped strontium ions. *Optics Communications*, 158:36–40, 1998.

[36] T. Stace, A.N. Luiten, and R.P. Kovacich. Laser offset-frequency locking using a frequency-to-voltage converter. *Meas. Scietific Technologies*, 9:1635–1637, 1998.

[37] H.N. Rutt. A heterodyne frequency offset locking technique for pulsed or cw lasers. *Journal of Physics E: Scientific Instruments*, 17:704–709, 1984.

[38] U. Schuenemann, H. Engler, R. Grimm, M. Weidemueller, and M. Zielonkowski. Simple scheme for tunable frequency offset locking of two lasers. *Review of Scientific Instruments*, 70:242–243, 1999.

[39] G. Ritt, G. Cennini, C. Geckeler, and M. Weitz. Laser frequency offset locking using a side of filter technique. *Applied Physics B*, 79:363–365, 2004.

[40] M.W. Hamilton. An introduction to stabilized lasers. *Contemporary Physics*, 30:21–33, 1989.

[41] P. Horowitz and W. Hill. *The Art of Electronics*. Cambridge University Press, New York, second edition, 1996.

[42] G. Thalhammer. Frequenzstabilisierung von Diodenlasern bei 850, 854 und 866 nm mit Linienbreiten im Kilohertz-Bereich. Master's thesis, Universität Innsbruck, 1999.

[43] U.L. Rohde, J. Whitaker, and T.T.N. Bucher. *Communications Receivers*. McGraw-Hill, second edition, 1997.

[44] A. Yariv. *Quantum Electronics*. John Wiley & Sons, Singapore, third edition, 1988.

Acknowledgements

Finally, I'd like to thank all the people that where somehow involved in this thesis and have been of help to finish it in time.

First of all, I'd like to thank Prof. Rainer Blatt as my supervisor. He cordially introduced me to the his group and had an eye on the progress of my work.

Special thanks go to the "Cavity Group": Christoph Becher, Carlos Russo, Eoin Phillips and Helena Barros. You are the first ones that I ask for help if I have screwed up something. No matter what, you always have an open ear for my problems.

At this point I have to announce, that I owe a lot to Eoin. He spent huge amounts of time to proofreading and correcting this thesis, until it finally had the form as you see it now. So, if you find any mistakes I'm the one to blame.

As I'll probably miss someone, I just want to thank the rest of the "Blatt Group" for discussions, help and jokes. You are the ones who create an atmosphere where I like to work.

Without telling names, I would like to thank all of my friends for keeping an eye on me. You have shared my feelings and have shown interest in what I do. What more can I ask for?

A cordial "Donk schian" goes to my parents, who made this study possible. While trusting in the path of life their son has chosen, they have been entertaining and accommodating all the time without asking a question.

Finally, I'd like to thank all of you (those mentioned and not-mentioned) again. You had the endurance to spend time, in the lab, office, mountains or somewhere else, with a very stubborn Tirolean, whose German is probably even worse than his English.

Curriculum Vitae

Thomas Monz
Auland 90
A-6103 Reith bei Seefeld
Born on 28th January 1981 in Hall in Tirol, Austria

Education and Professional training:

2004–2005	Diploma thesis under the guidance of Prof. Blatt, Department of Experimental Physics, University of Innsbruck: *"A Frequency Offset Lock for Cavity-Driven Raman Transitions"*.
2000–2005	Diploma study at the University of Innsbruck. *Master of Natural Science (Magister Rerum Naturalium)* in Physics.
1999–2000	Military service at 1.Pi/B.2, Schwarzenbergkaserne, Salzburg
1991–1999	Highschool Sillgasse, Innsbruck. *Matura (22.6.1999).*